Electronic Supplementary Information

Regulating the allocation of N and P in codoped graphene *via* supramolecular control to remarkably boost hydrogen evolution

Hao Wu,[a] *Zhimin Chen,**[a] *Ying Wang,*[a] *Erping Cao,*[a] *Fei Xiao,*[a] *Shuo Chen,*[a] *Shichao Du,*[a] *Yiqun Wu**[ab] *and Zhiyu Ren**[a]

[a] Key Laboratory of Functional Inorganic Material Chemistry (Ministry of Education of China), School of Chemistry and Materials Science, Heilongjiang University, 74# Xuefu Road, Nangang District, Harbin 150080, People's Republic of China;

[b] Shanghai Institutes of Optics and Fine Mechanics, Chinese Academy of Sciences, 390# Qinghe Road, Jiading District, Shanghai 201800, People's Republic of China.

* Corresponding author E-mail: zmchen@hlju.edu.cn; yqwu@siom.ac.cn; zyren@hlju.edu.cn.

Tel.: +86 451 86604331,

Fax: +86 451 86608616.

Table of contents

1. Supplementary Figures

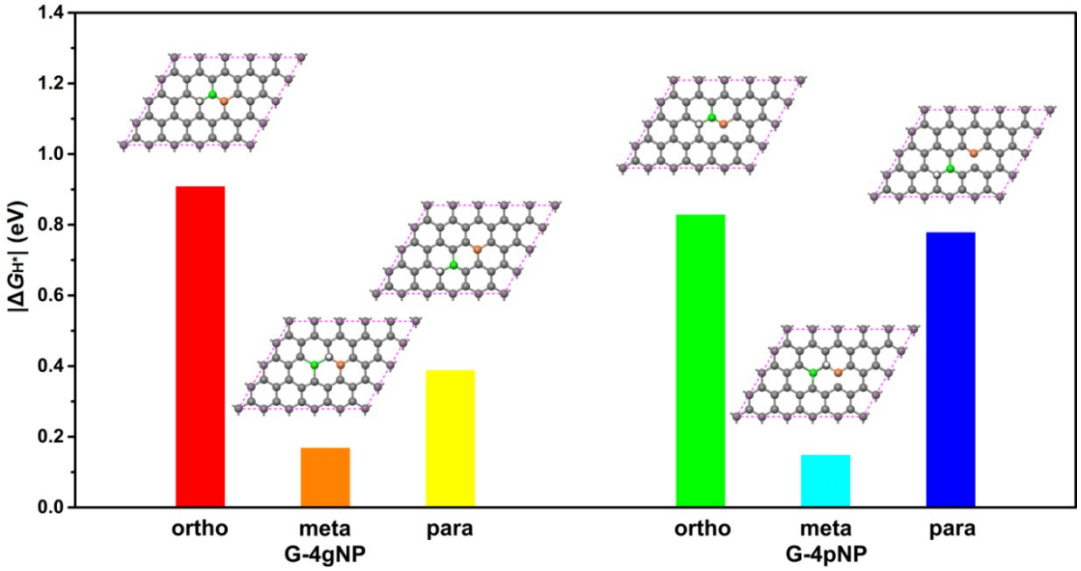

Fig. S1. $|\Delta G_{H*}|$ and active sites (inset) on different N, P codoped graphene configurations with gN or pN groups. Ortho, Meta, Para indicates the relative positions of N and P heteroatoms in one benzene heteroring. The grey, orange, green and white balls represent C, N, P and H atoms, respectively, and the unit cells of various models are indicated by pink dashed line.

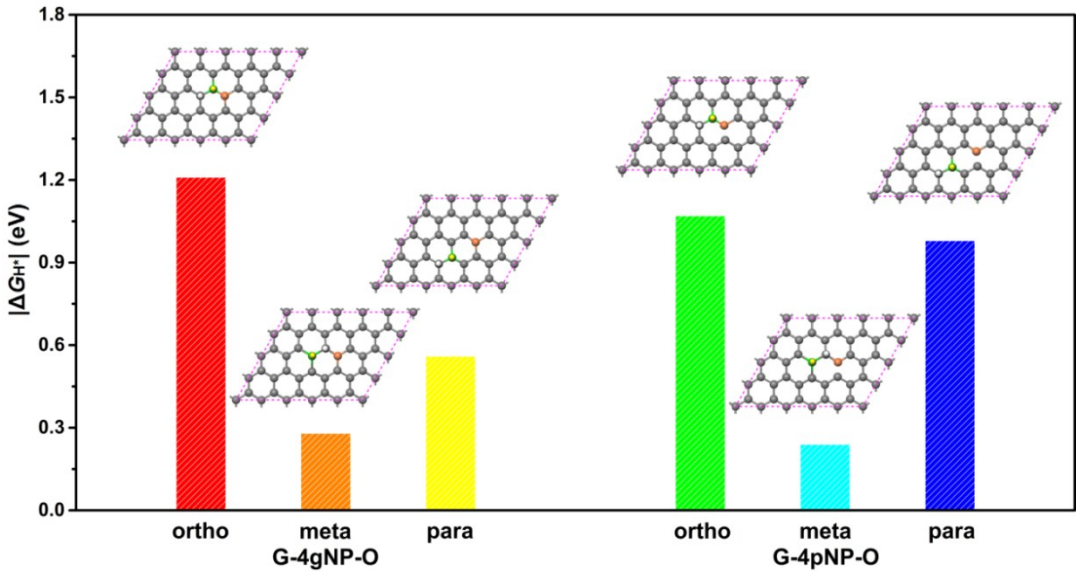

Fig. S2. $|\Delta G_{H*}|$ and active sites (inset) on different N, P-O codoped graphene configurations with gN or pN groups. Ortho, Meta, Para indicates the relative positions of N and P-O heteroatoms in one benzene heteroring. The grey, orange, green, yellow and white balls represent C, N, P, O and H atoms, respectively, and the unit cells of various models are indicated by pink dashed line.

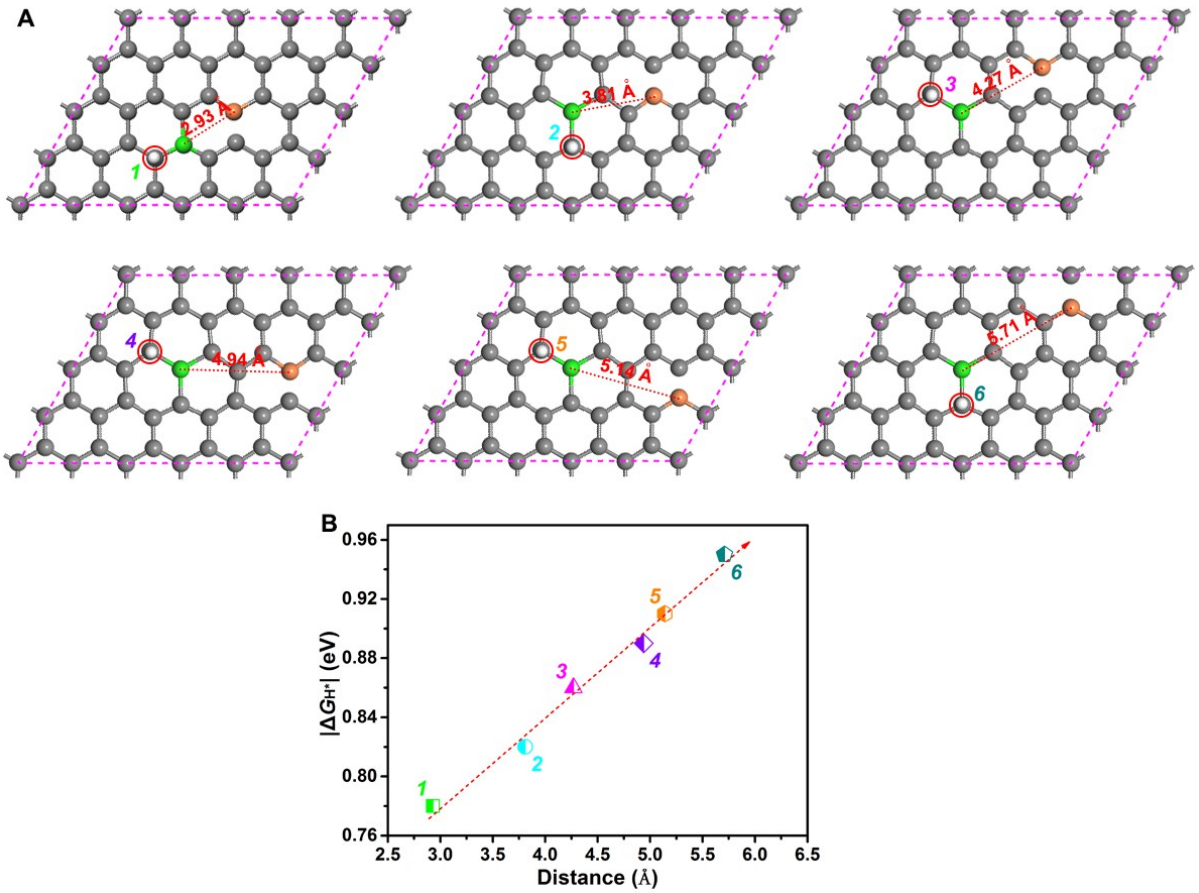

Fig. S3. (A) The optimized models of various G-4pNP, in which the most active of hydrogen adsorption sites are indicated by a red circle, the distance between pN and P doping is marked by red dot lines, the grey, orange, green and white balls represent C, N, P and H atoms, respectively, and the unit cells of various models are indicated by pink dashed line. (B) The corresponding $|\Delta G_{H^*}|$ values of various G-4pNP.

The corresponding calculated results shown in ***Fig. S3*** indicate that the $|\Delta G_{H^*}|$ value of the most active C site becomes larger gradually with increasing the distance between N and P heteroatoms.

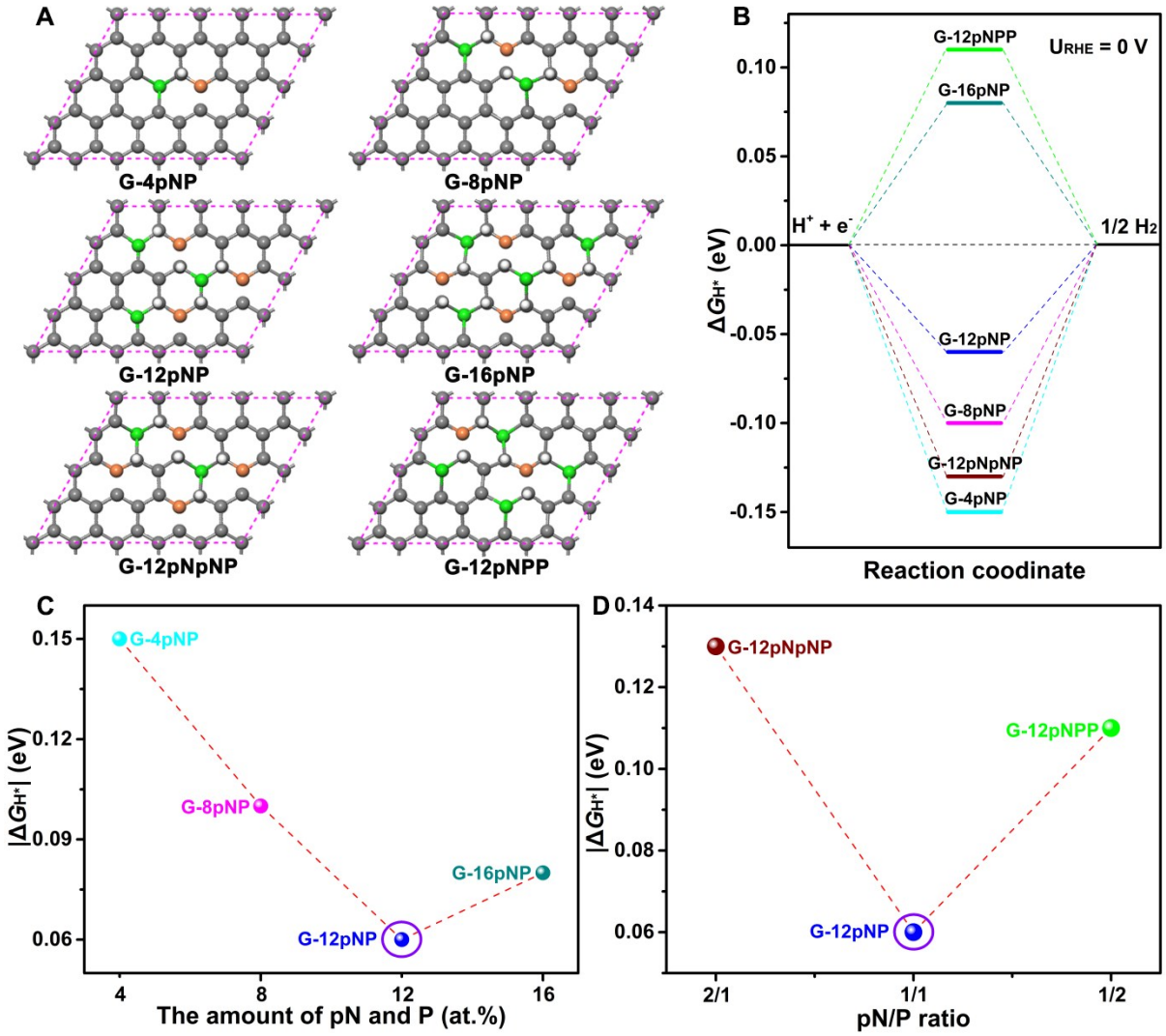

Fig. S4. (A) Hydrogen adsorption sites and configurations on different G-pNP models. The grey, orange, green and white balls represent C, N, P and H atoms, respectively, and the unit cells of various models are indicated by pink dashed line. (B) The calculated free energy (ΔG_{H*}) diagram for HER at the equilibrium potential (U_{RHE} = 0 V) of different G-pNP models. (C) The $|\Delta G_{H*}|$ value of G-pNP with different amount of pN and P (the pN/P equals 1/1). (D) The $|\Delta G_{H*}|$ value of G-pNP with different pN/P ratio (the amount of pN and P equals 12 at.%). The hydrogen adsorption sites and configurations on different pN, P codoped graphene (G-pNP) models are depicted in ***Fig. S4A***, in which G-pNP with pN/P equals 1/1 and X at.% (X = 4, 8, 12, and 16) of pN and P are abbreviated as G-4pNP, G-8pNP, G-12pNP and G-16pNP; G-pNP with 12 at.% of pN and P at pN/P equals 2:1 or 1:2 are abbreviated as G-12pNpNP and G-12pNPP.

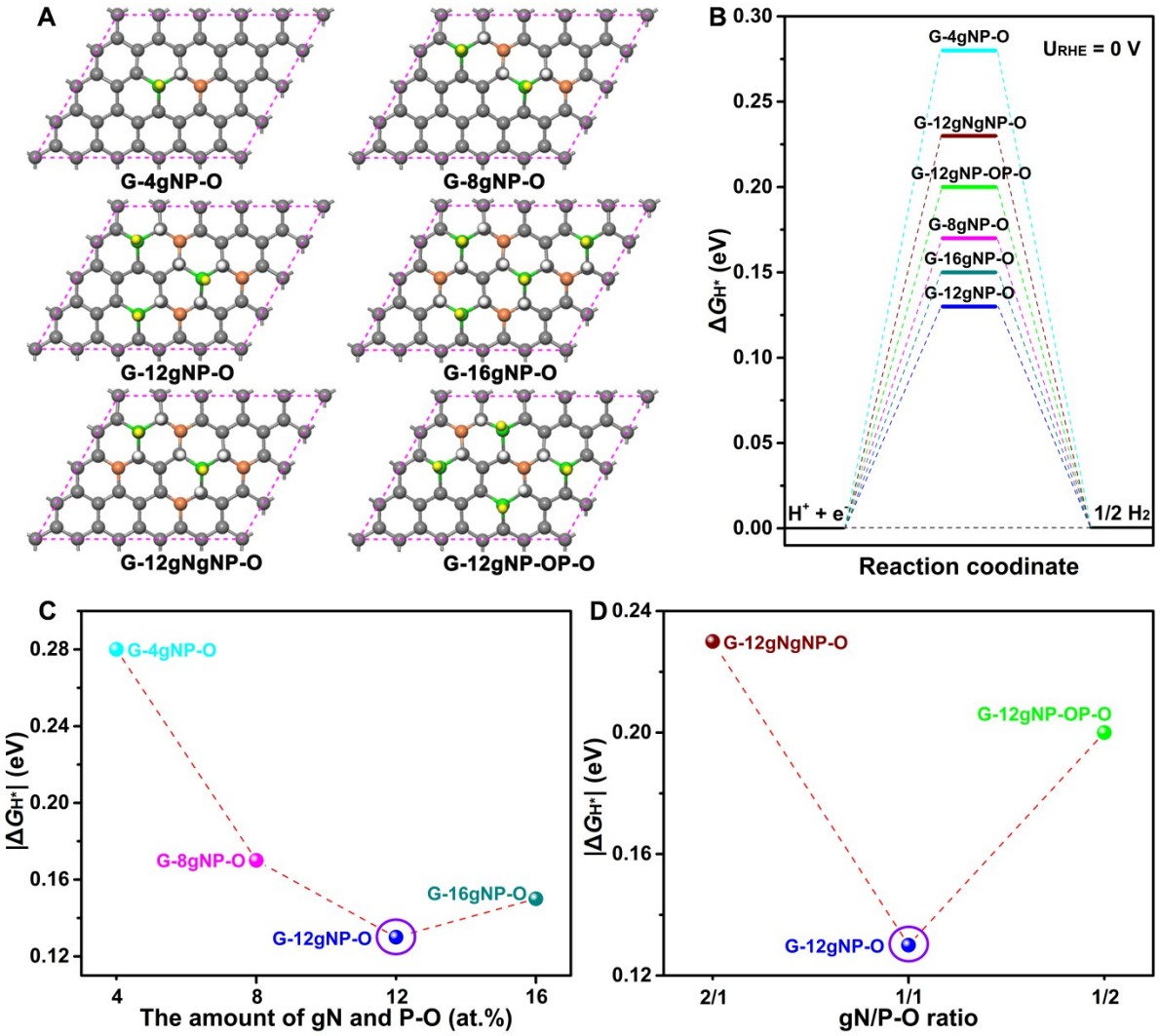

Fig. S5. (A) Hydrogen adsorption sites and configurations on different G-gNP-O models. The grey, orange, green, yellow and white balls represent C, N, P, O and H atoms, respectively, and the unit cells of various models are indicated by pink dashed line. (B) The calculated free energy (ΔG_{H*}) diagram for HER at the equilibrium potential (U_{RHE} = 0 V) of different G-gNP-O models. (C) The $|\Delta G_{H*}|$ value of G-gNP-O with different amount of gN and P-O (the gN/P-O equals 1/1). (D) The $|\Delta G_{H*}|$ value of G-gNP-O with different gN/P-O ratio (the amount of gN and P-O equals 12 at.%). The hydrogen adsorption sites and configurations on different gN, P-O codoped graphene (G-gNP-O) models are depicted in ***Fig. S5A***, in which G-gNP-O with gN/P-O equals 1/1 and X at.% (X = 4, 8, 12, and 16) of gN and P-O are abbreviated as G-4gNP-O, G-8gNP-O, G-12gNP-O and G-16gNP-O; G-gNP-O with 12 at.% of gN and P-O at gN/P-O equals 2:1 or 1:2 are abbreviated as G-12gNgNP-O and G-12gNP-OP-O.

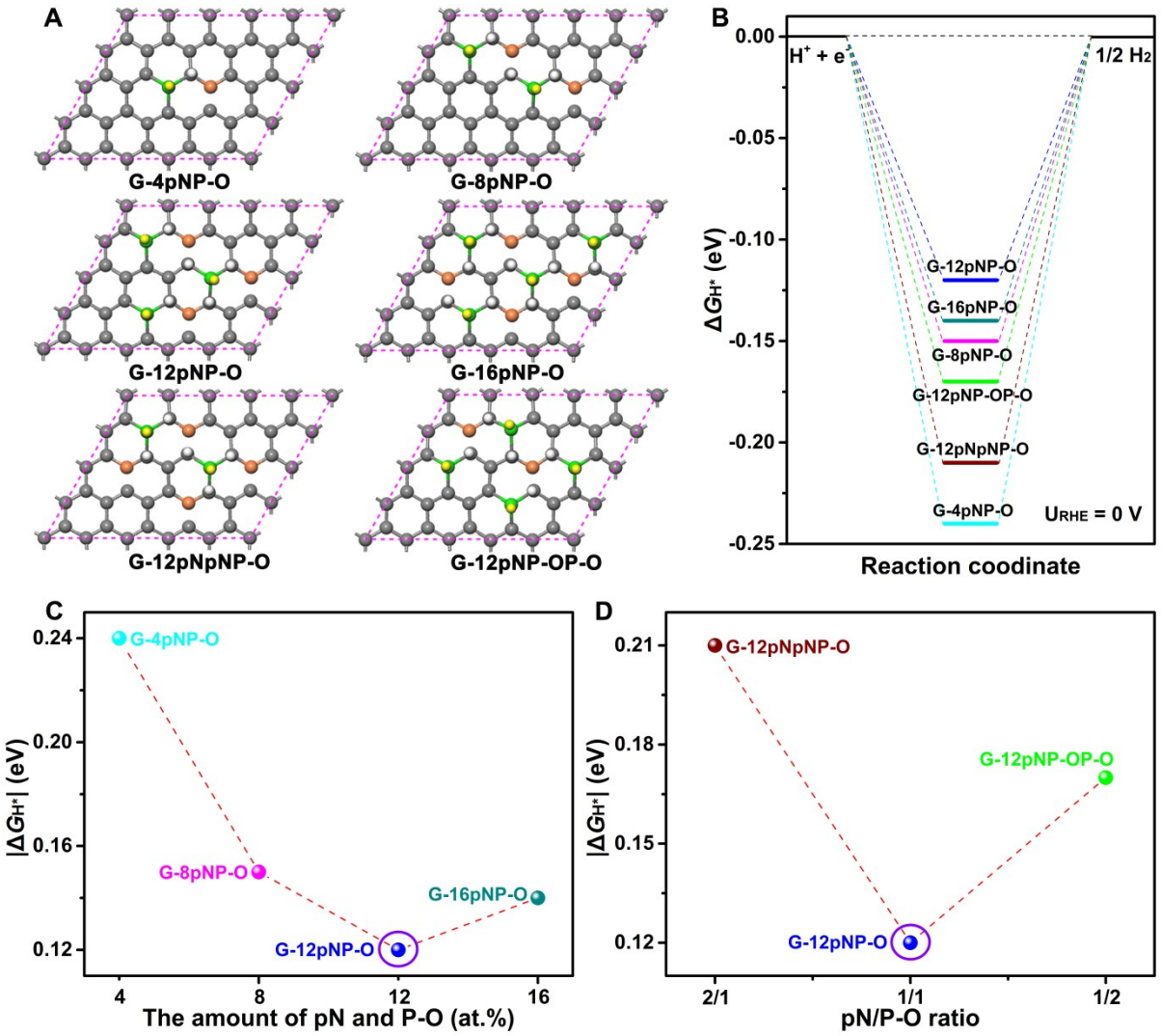

Fig. S6. (A) Hydrogen adsorption sites and configurations on different G-pNP-O models. The grey, orange, green, yellow and white balls represent C, N, P, O and H atoms, respectively, and the unit cells of various models are indicated by pink dashed line. (B) The calculated free energy (ΔG_{H*}) diagram for HER at the equilibrium potential (U_{RHE} = 0 V) of different G-pNP-O models. (C) The $|\Delta G_{H*}|$ value of G-pNP-O with different amount of pN and P-O (the pN/P-O equals 1/1). (D) The $|\Delta G_{H*}|$ value of G-pNP-O with different pN/P-O ratio (the amount of pN and P-O equals 12 at.%). The hydrogen adsorption sites and configurations on different pN, P-O codoped graphene (G-pNP-O) models are depicted in ***Fig. S6A***, in which G-pNP-O with pN/P-O equals 1/1 and X at.% (X = 4, 8, 12, and 16) of pN and P-O are abbreviated as G-4pNP-O, G-8pNP-O, G-12pNP-O and G-16pNP-O; G-pNP-O with 12 at.% of pN and P-O at pN/P-O equals 2:1 or 1:2 are abbreviated as G-12pNpNP-O and G-12pNP-OP-O.

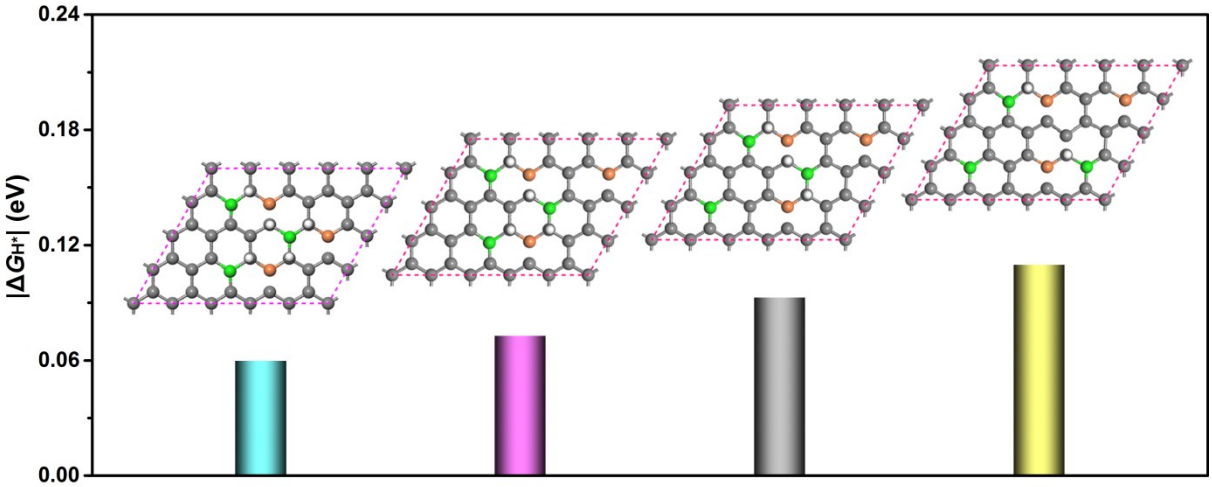

Fig. S7. The $|\Delta G_{H*}|$ values of G-12pNP with different heteroatom's distribution. The grey, orange, green and white balls represent C, N, P and H atoms, respectively, and the unit cells of various models are indicated by pink dashed line.

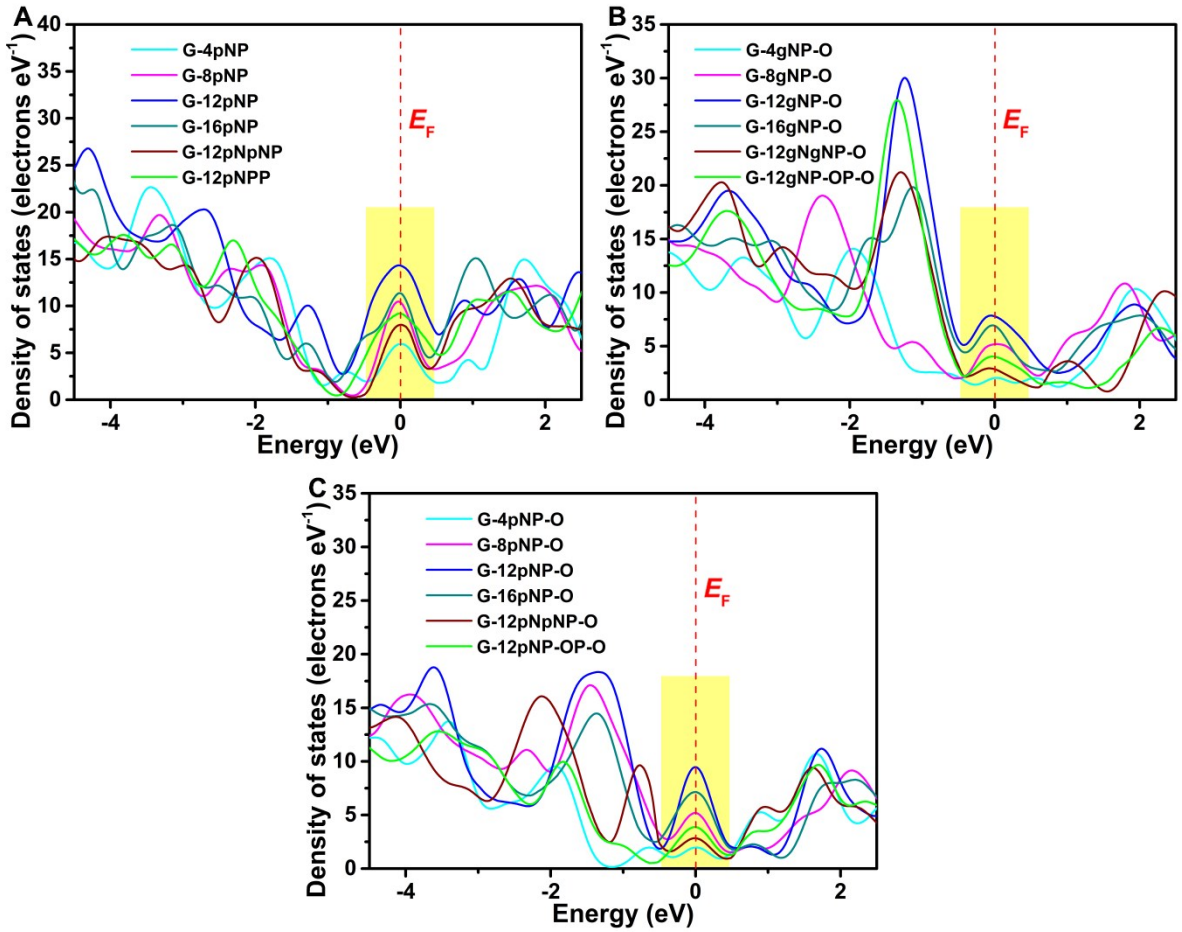

Fig. S8. The DOS plots of different G-pNP (A), G-gNP-O (B) and G-pNP-O (C) models.

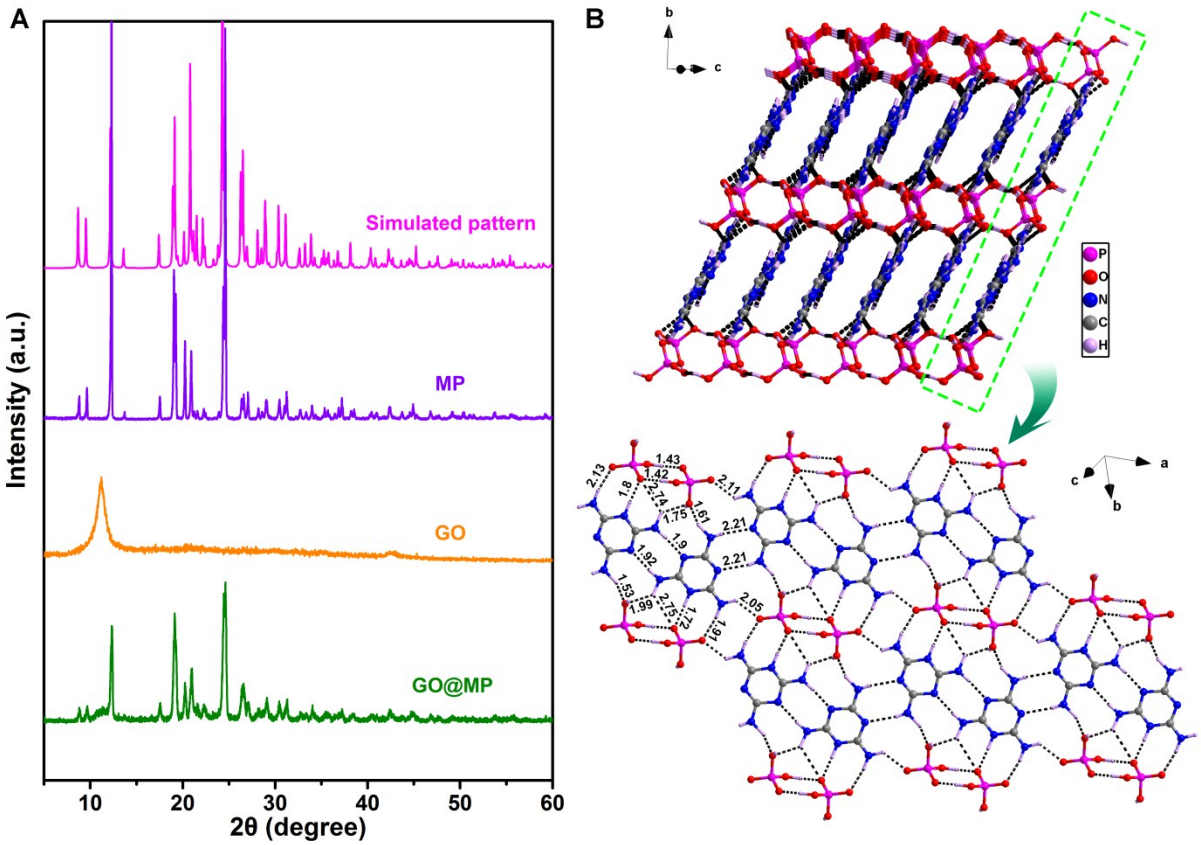

Fig. S9. (A) Simulated pattern of MP supramolecular assemblies based on single crystal data of previous report[S1], and measured powder XRD patterns of MP, GO and GO@MP, respectively. (B) Packing diagram and corresponding H-bonded network of MP derived from the deposited cif-file in CCDC (No. 224290), where the dashed lines represent H-bonds.

As shown in ***Fig. S9A***, sharp peaks in XRD pattern of the obtained MP agrees well with the simulated pattern, indicating that melamine and phosphoric acid have successfully assembled together and formed the ordered supramolecular architecture based on H-bonds (***Fig. S9B***). Moreover, GO@MP contains all the XRD peaks corresponding to MP and GO, confirming the successful assembly between MP and GO.

References:

S1. D. J. A. De Ridder, K. Goubitz, V. Brodski, R. Peschar and H. Schenk, *Helvetica Chimica Acta*, 2004, **87**, 1894-1905.

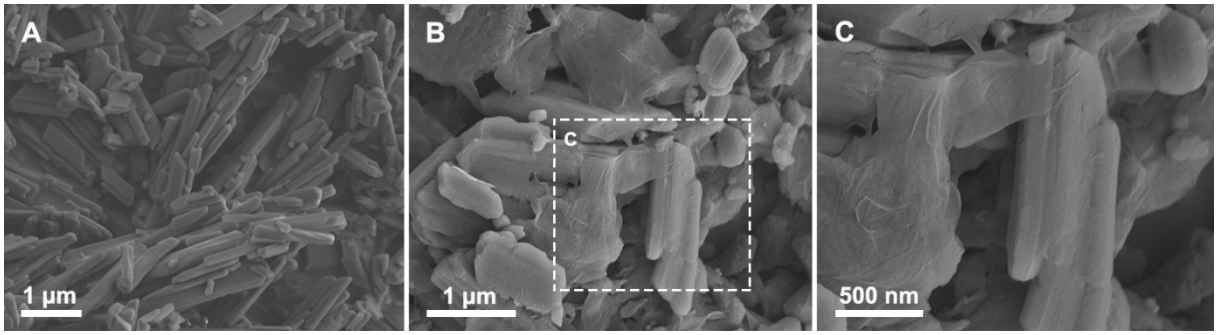

Fig. S10. SEM images of MP (A) and rGO/MP (B and C).

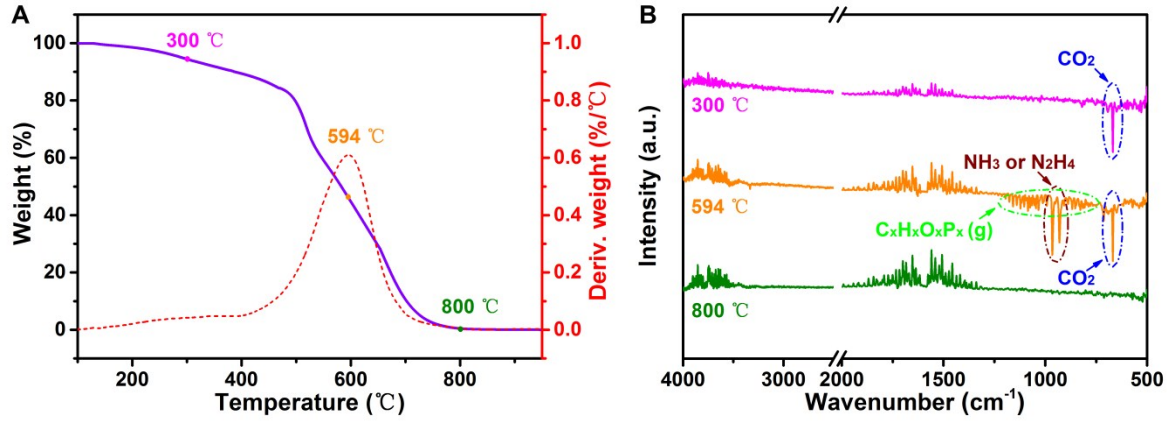

Fig. S11. TGA and DTG curves of MP measured under N_2 atmosphere (A) and the temperature-dependent evolution of the FTIR spectra of the corresponding gaseous products released at decomposition temperatures of 300, 594 and 800 °C (B).

As shown in ***Fig. S11A***, a great loss of weight appears in the TGA curve of MP accompanied by the increasing of temperature. The loss of weight at 700 ºC is about 89.45 %. And, when the temperature goes up to 900 ºC, only a negligible MP residue (about 0.06 %) is observed. Therefore, after treating the GO@MP at 900 ºC for 2 h under N_2 atmosphere, MP on the surface of GO can be gasified almost completely. During the pyrolysis, the decomposition of MP releases a large amount of gas (*e.g.*, CO_2, NH_3, N_2H_4 and $C_xH_xO_xP_x$) from the interlayer space of graphene nanosheets (***Fig. S11B***), which consequently produces substantial internal stresses, leading to the expansion of graphene nanosheets to suppress the stacking.

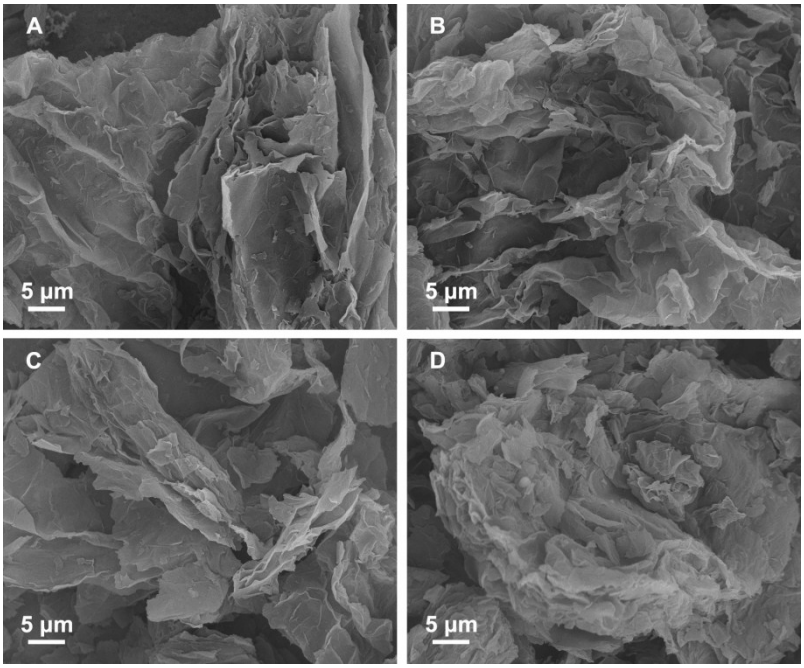

Fig. S12. SEM images of G-12NP-700 (A), G-12NP (B), G-12NP-1000 (C) and GO-900 (D).

As shown in ***Fig. S12A-C***, G-12NP-700, G-12NP and G-12NP-1000 exhibit a crumpled and loose-packed thin layer. By contrast, the thermally reduced GO (GO-900) with the absence of MP tends to aggregate, forming a graphite-like structure (***Fig. S12D***).

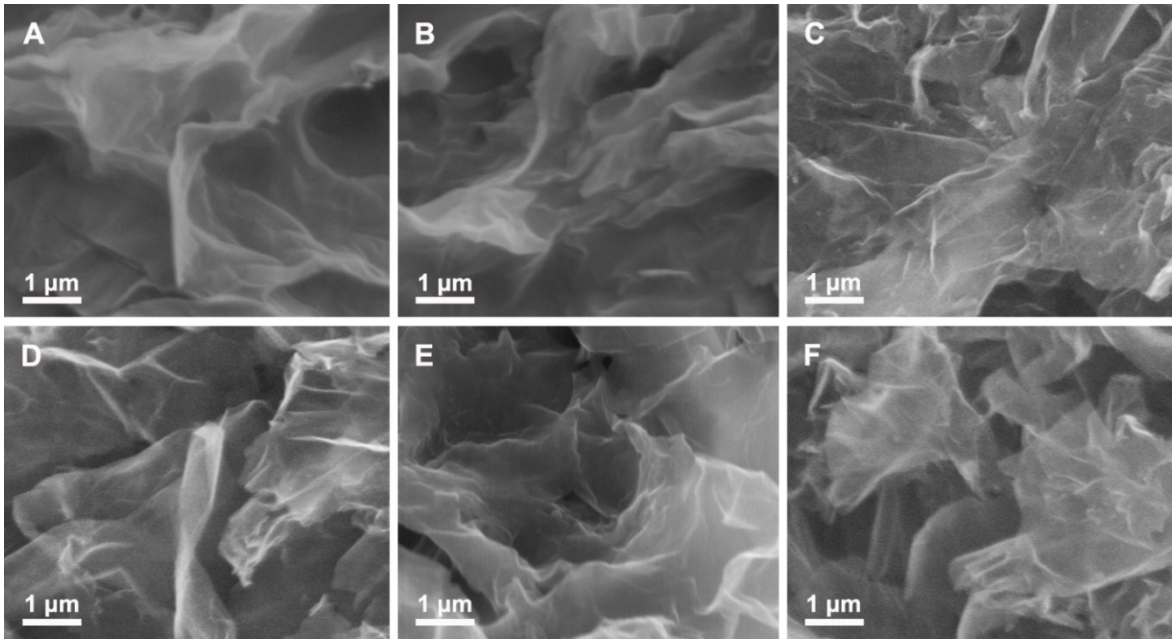

Fig. S13. SEM images of G-4NP (A), G-8NP (B), G-12NP (C), G-16NP (D), G-12NNP (E) and G-12NPP (F).

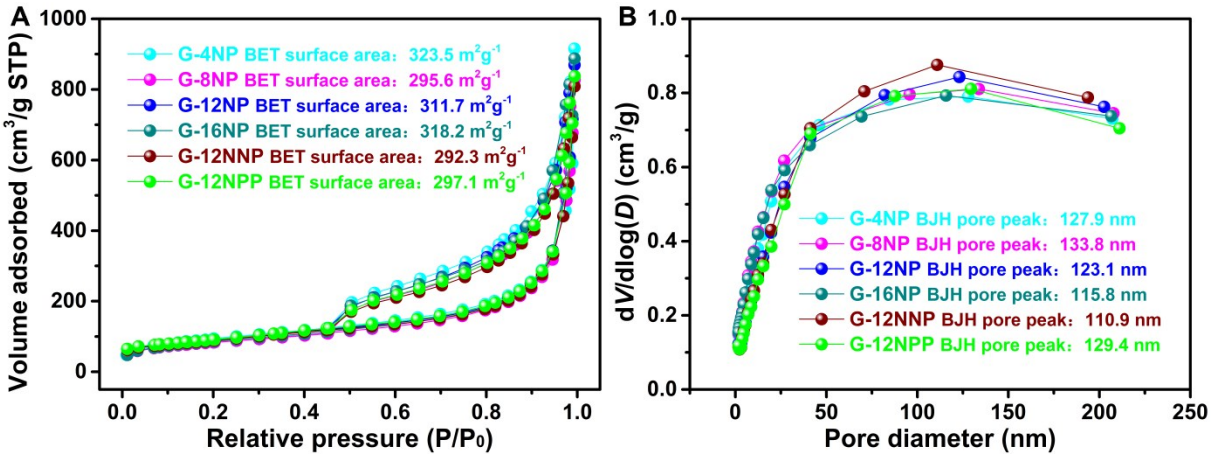

Fig. S14. N_2 adsorption-desorption isotherms (A) and pore-size distribution curves (B) of G-4NP, G-8NP, G-12NP, G-16NP, G-12NNP and G-12NPP.

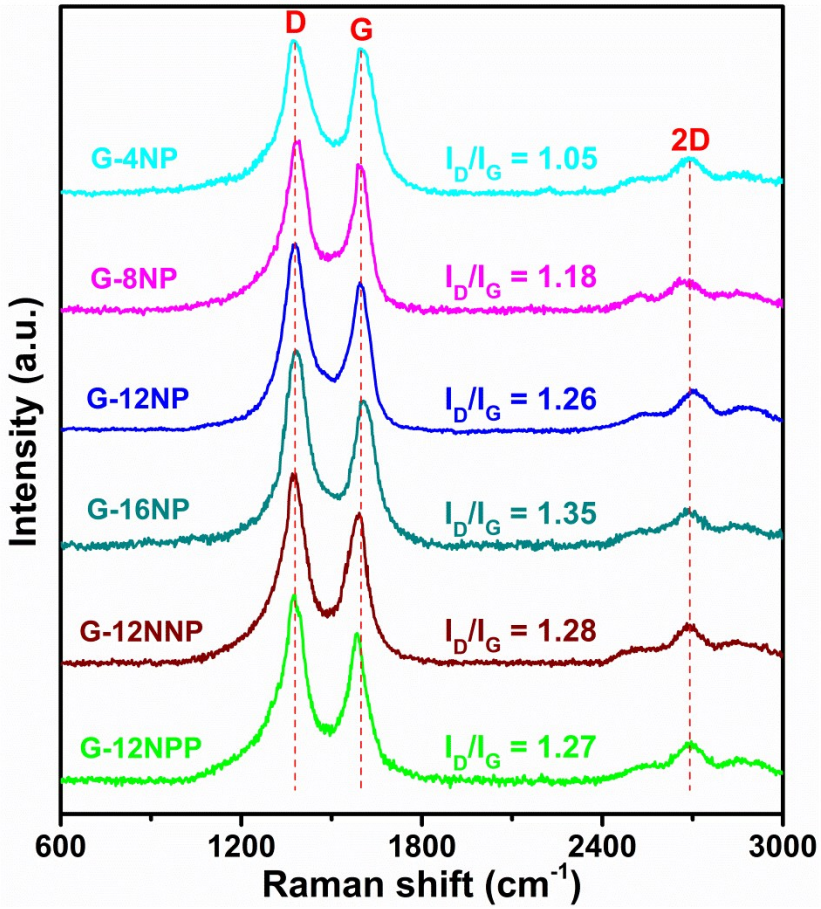

Fig. S15. Raman spectra of G-4NP, G-8NP, G-12NP, G-16NP, G-12NNP and G-12NPP obtained at λ_{exc} = 457.9 nm.

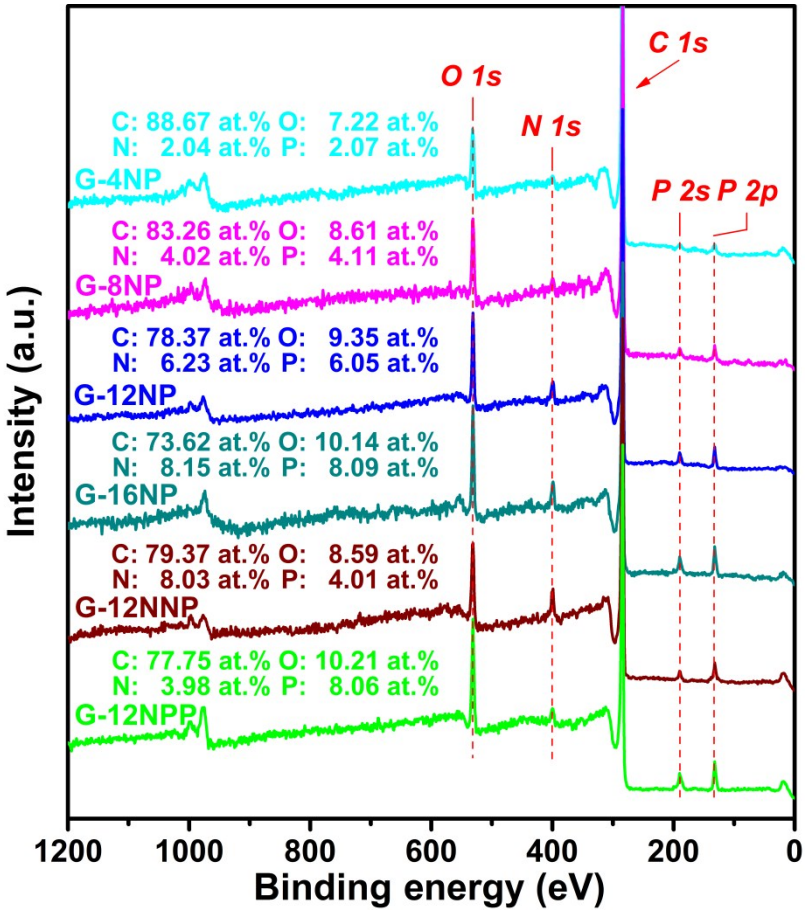

Fig. S16. Survey XPS spectra of G-4NP, G-8NP, G-12NP, G-16NP, G-12NNP and G-12NPP.

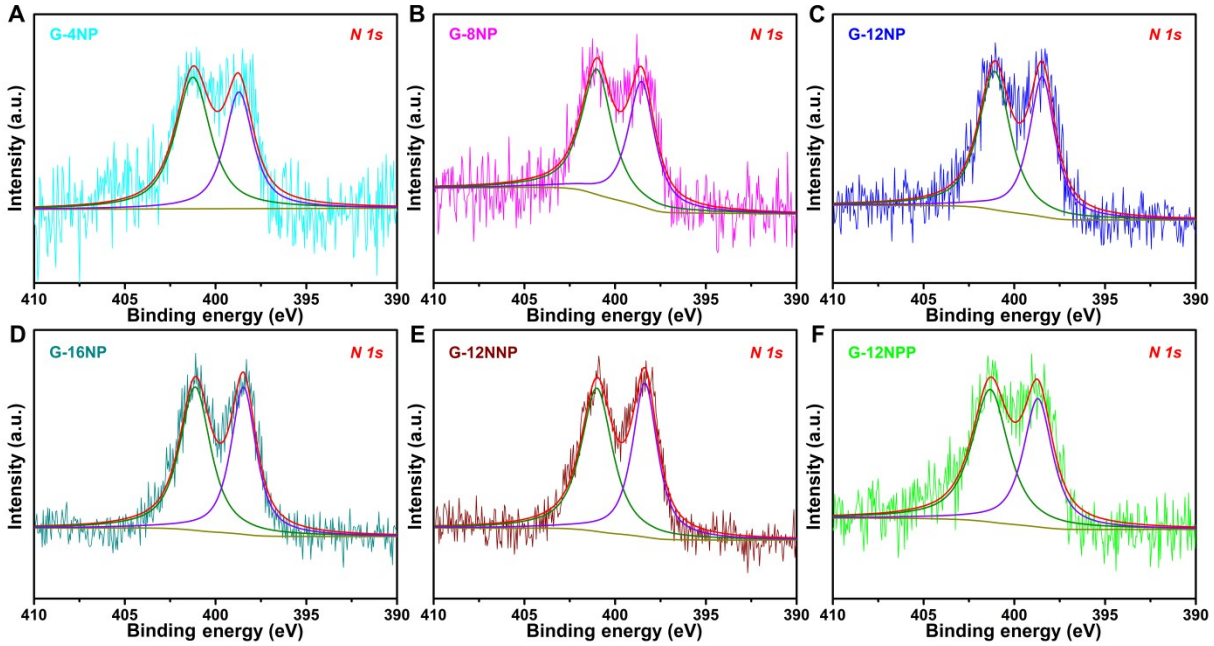

Fig. S17. The high-resolution N *1s* XPS spectra obtained for G-4NP, G-8NP, G-12NP, G-16NP, G-12NNP and G-12NPP.

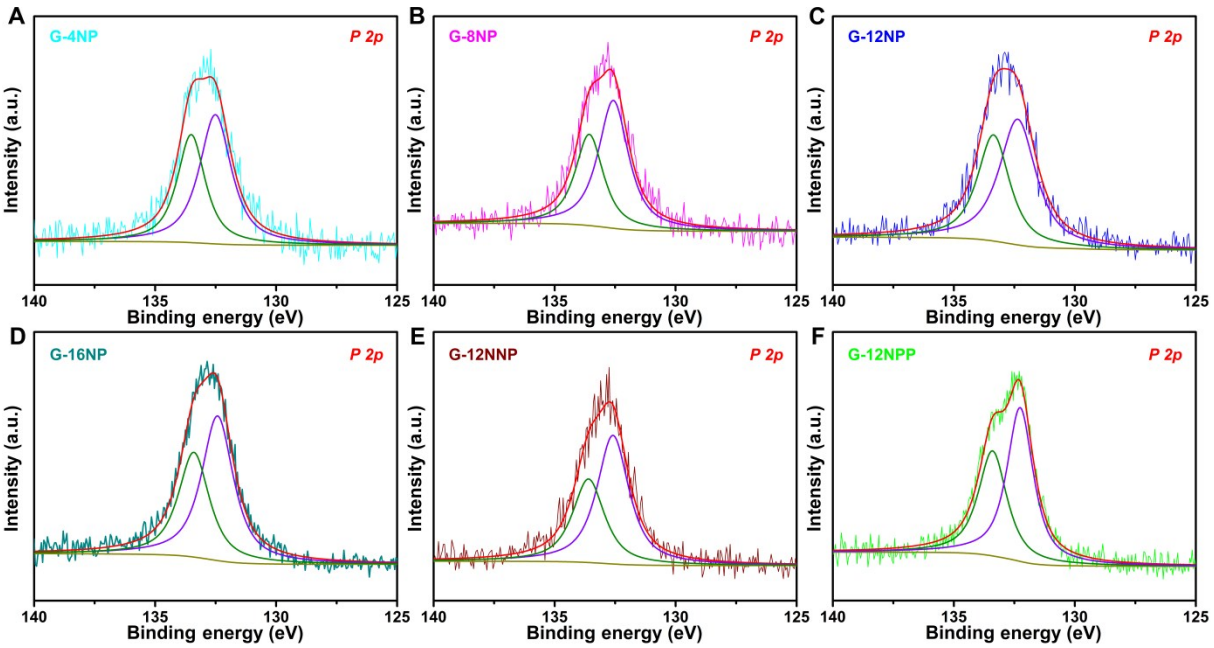

Fig. S18. The high-resolution P *2p* XPS spectra obtained for G-4NP, G-8NP, G-12NP, G-16NP, G-12NNP and G-12NPP.

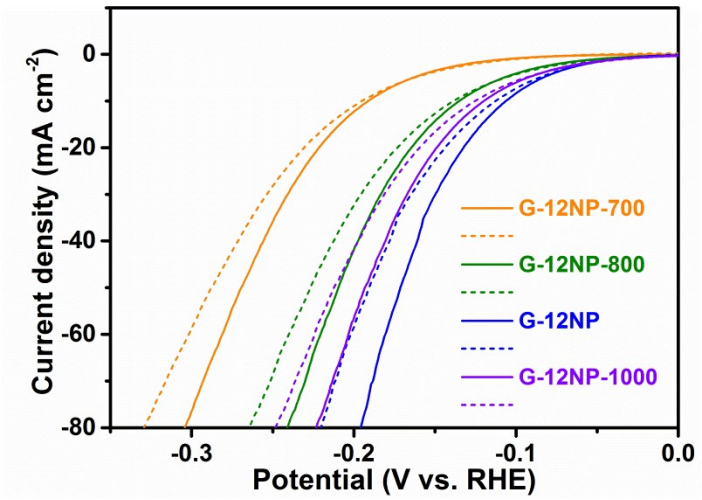

Fig. S19. HER polarization curves of G-12NP-700, G-12NP-800, G-12NP and G-12NP-1000 in 0.5 M H_2SO_4 with (solid lines) and without *iR* correction (dashed lines).

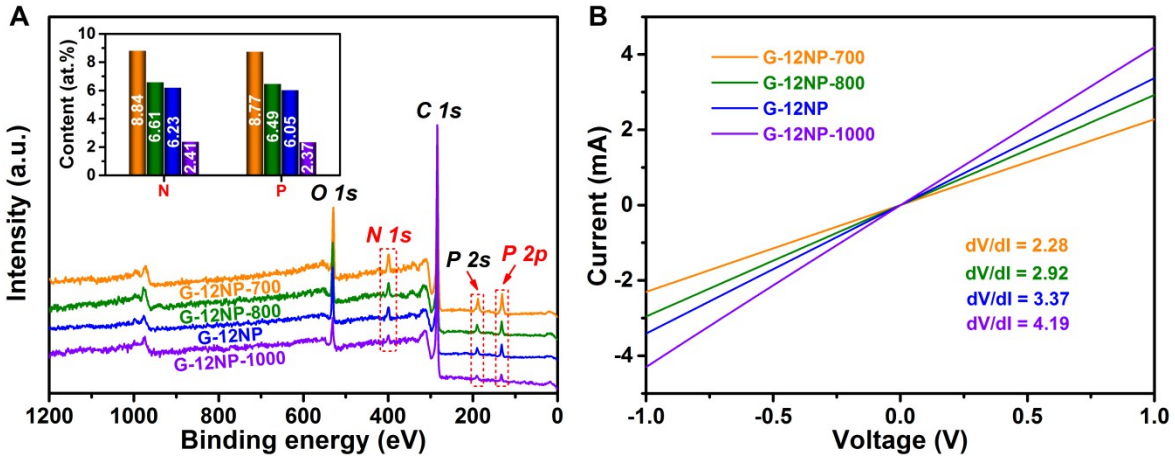

Fig. S20. (A) The survey XPS spectra of G-12NP-700, G-12NP-800, G-12NP and G-12NP-1000. The inset in (A) is the corresponding atomic percentages of N and P. (B) *I*−*V* curves of G-12NP-700, G-12NP-800, G-12NP and G-12NP-1000.

To determine the doping level and evaluate the conductivity of G-12NP-700, G-12NP-800, G-12NP and G-12NP-1000 prepared at 700, 800, 900 and 1000 ºC, respectively, XPS and *I*−*V* characteristics measurements were performed. As shown in ***Fig. S20***, the atomic percentages of N and P decreases in the order of G-12NP-700 > G-12NP-800 > G-12NP > G-12NP-1000 (***Fig. S20A***) and the dV/dI values increases in the order of G-12NP-700 < G-12NP-800 < G-12NP < G-12NP-1000 (***Fig. S20B***). The appropriate pyrolysis temperature of 900 ºC can balance the two factors in HER, the heteroatom-doping amount and the conductivity of G-NP.

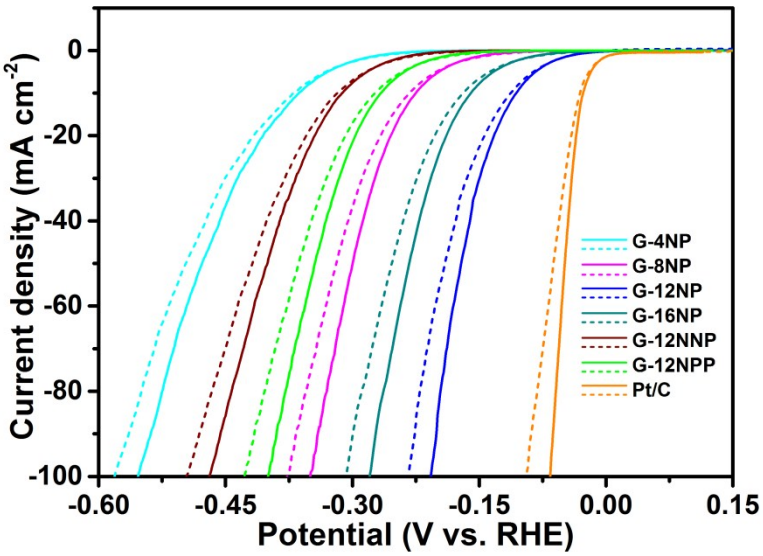

Fig. S21. HER polarization curves of various G-NP and Pt/C in 0.5 M H_2SO_4 with (solid lines) and without *iR* correction (dashed lines).

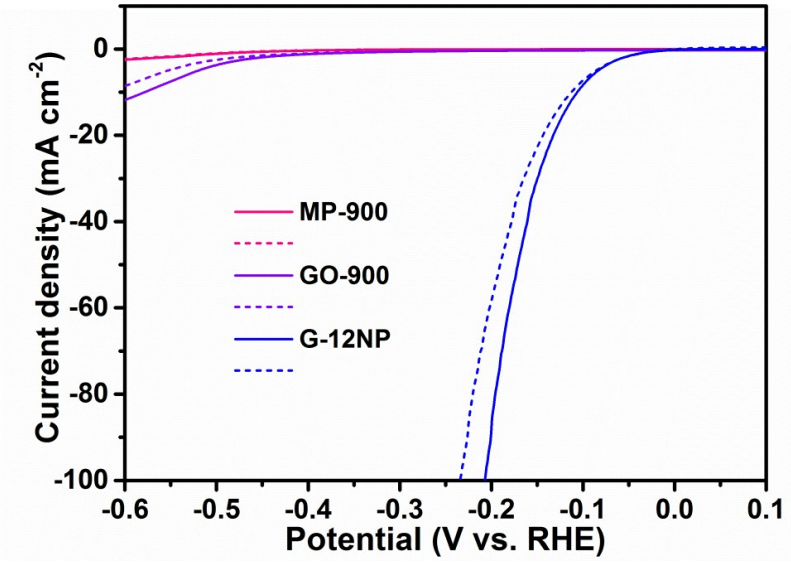

Fig. S22. HER polarization curves of MP-900, GO-900 and G-12NP in 0.5 M H_2SO_4 with (solid lines) and without *iR* correction (dashed lines).

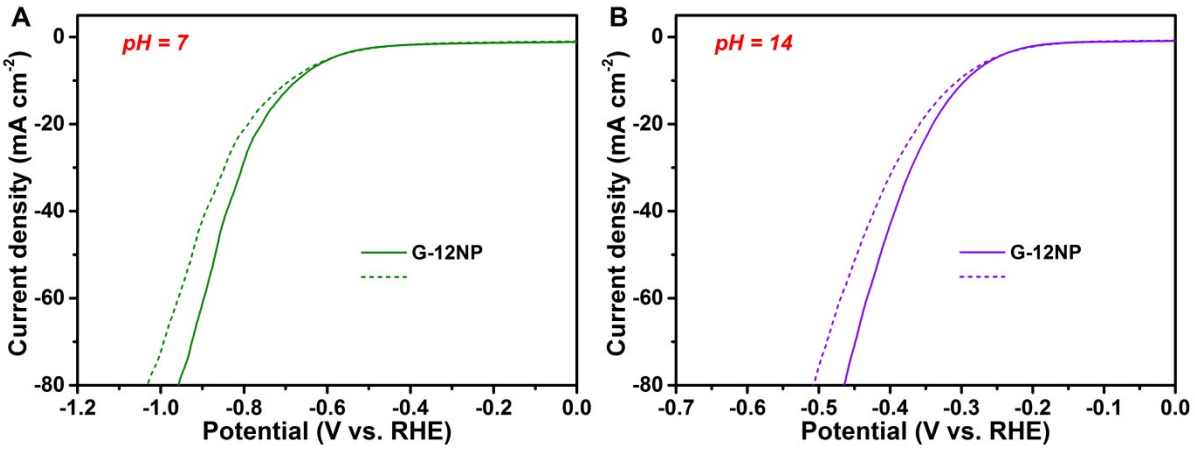

Fig. S23. HER polarization curves of G-12NP with (solid lines) and without *iR* correction (dashed lines) in H_2-saturated 0.5 M PBS (A) and 1 M KOH (B), respectively.

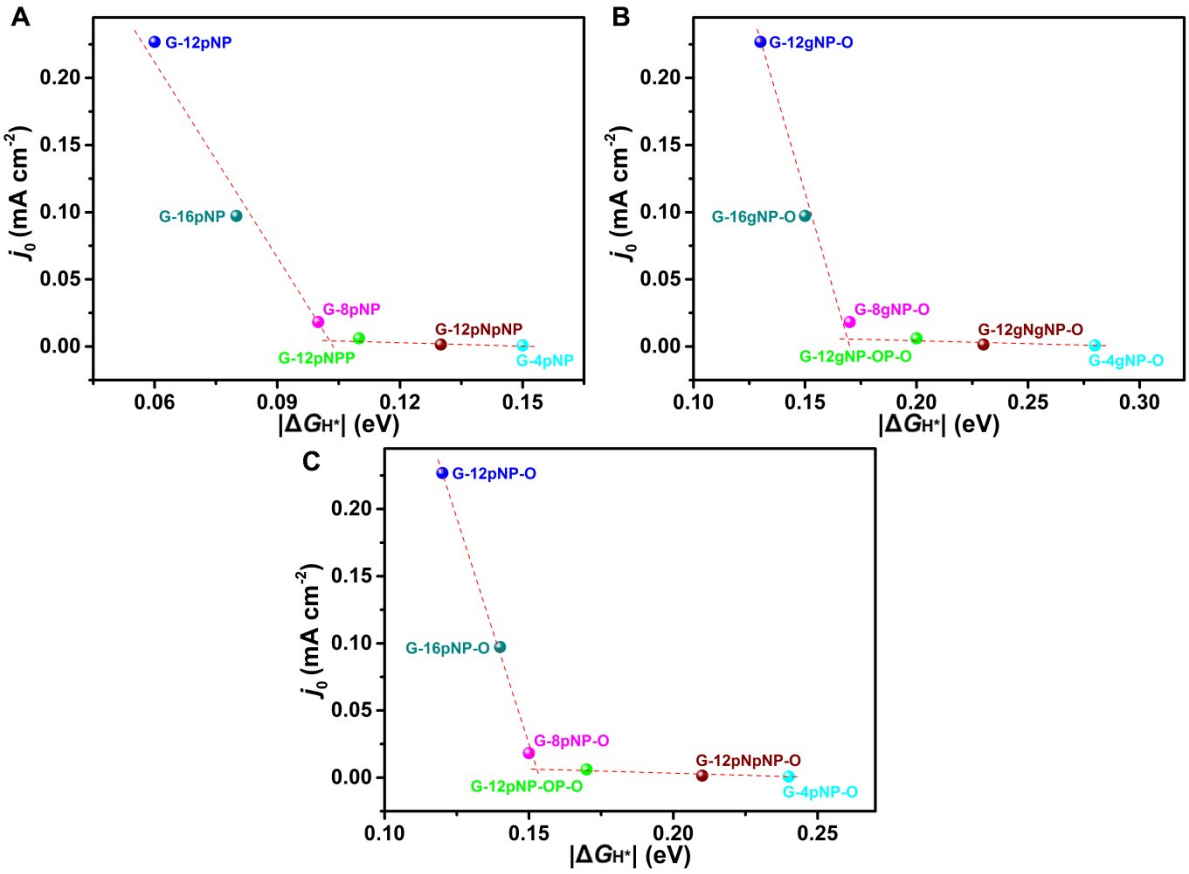

Fig. S24. Relationships between the j_0 of the produced G-NP and the $|\Delta G_{H*}|$ of different G-pNP (A), G-gNP-O (B) and G-pNP-O (C) models.

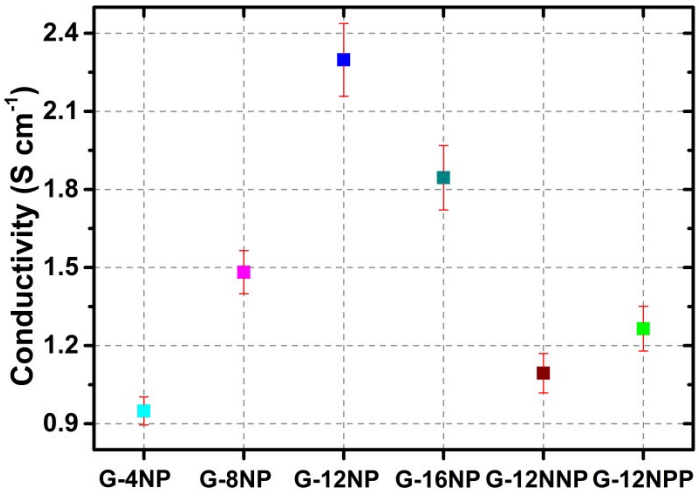

Fig. S25. Conductivity of various G-NP catalysts measured by 4-point probe method.

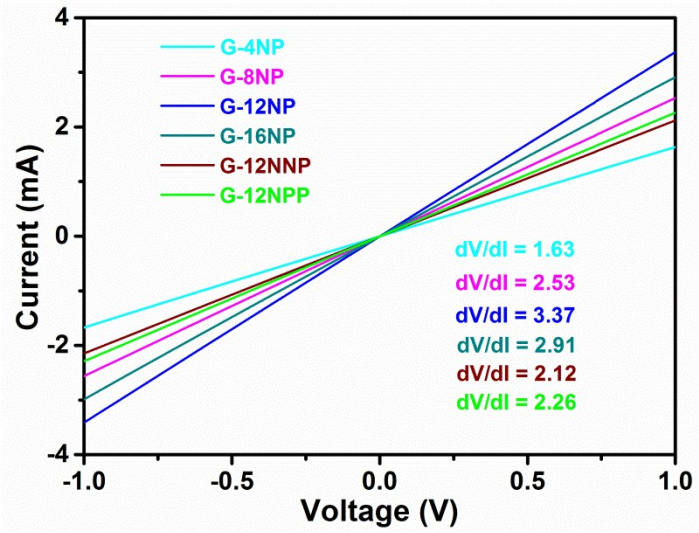

Fig. S26. *I*−*V* curves of various G-NP catalysts.

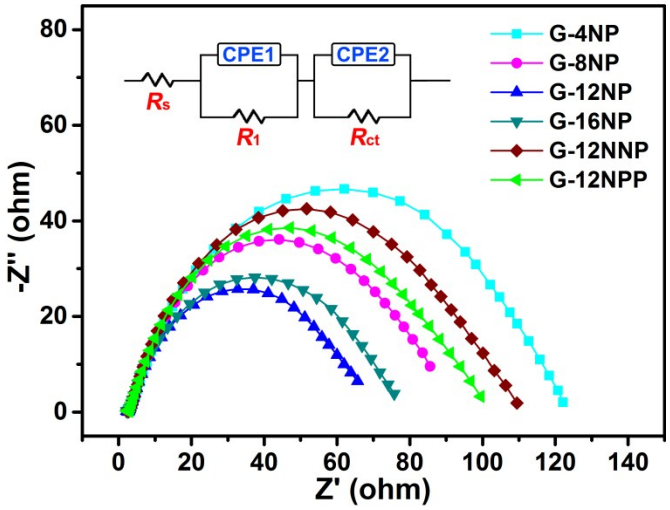

Fig. S27. Nyquist plots of various G-NP catalysts, the inset is the equivalent circuit model applied to fit the Nyquist plots, where R_s is the electrolyte resistance, R_1 relates to the interfacial resistance resulting from the electron transport between the catalyst and the GCE, R_{ct} is the charge-transfer resistance and CPE1 and CPE2 represent the double layer capacitance.

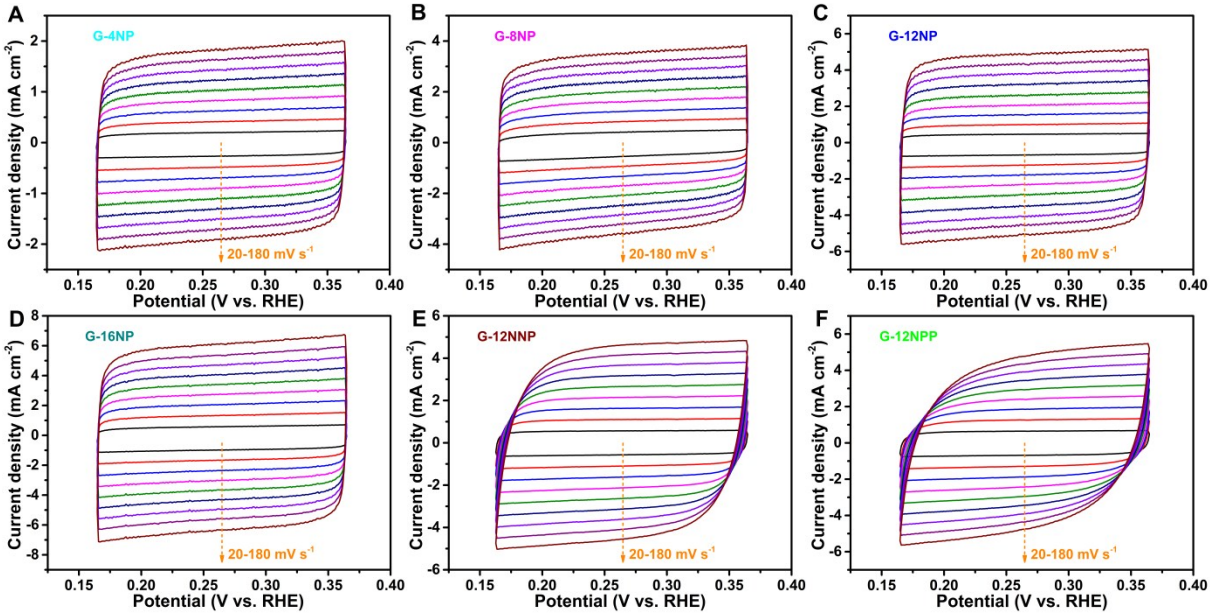

Fig. S28. CVs for G-4NP (A), G-8NP (B), G-12NP (C), G-16NP (D), G-12NNP (E) and G-12NPP (F) at different scan rate from 20 to 180 mV s^{-1}.

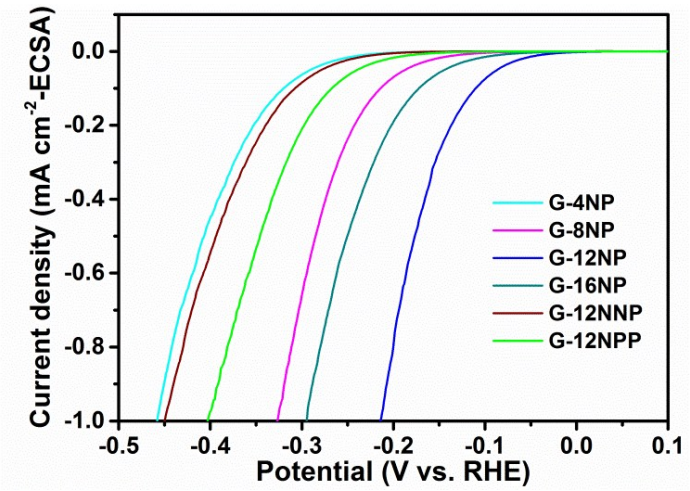

Fig. S29. *iR*-compensated HER polarization curves of various G-NP catalysts with current densities normalized to ECSA in 0.5 M H_2SO_4.

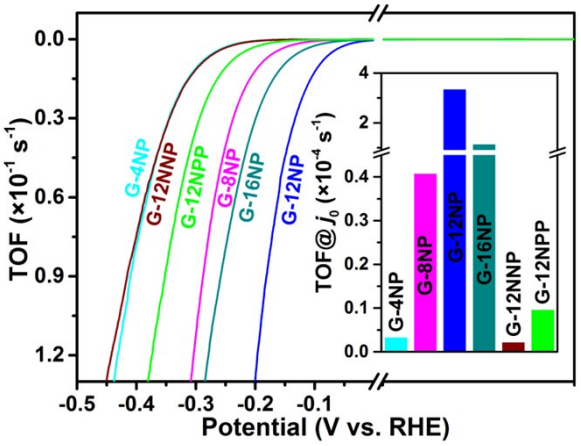

Fig. S30. TOFs of various G-NP catalysts in 0.5 M H_2SO_4, the inset is the corresponding TOF value required for the $j = j_0$.

The TOFs of various G-NP catalysts in 0.5 M H_2SO_4 for the HER is calculated by the equation:

$$TOF = \frac{Total\ number\ of\ hydrogen\ turnover/geometric\ area\ (cm^2)}{Number\ of\ active\ sites/geometric\ area\ (cm^2)}$$

Total number of hydrogen turnover[S2,S3]

$$= (j\ mA\ cm^{-2})\left(\frac{1\ C\ s^{-1}}{10^3\ mA}\right)\left(\frac{1\ mol\ e^-}{96485.3\ C}\right)\left(\frac{1\ mol\ H_2}{2\ mol\ e^-}\right)\left(\frac{6.022\ \times 10^{23}\ molecules\ H_2}{1\ mol\ H_2}\right) = per\ mA\ cm^{-2}$$

The number of active sites is assumed to be equal to the number of heteroatoms (N and P) and all of these sites are accessible to the electrolyte. The real number of active and accessible sites should be considerably lower than the calculated value since the C atoms only between meta-type N and P in the heterocycles are the most potentially active site based on our DFT results. The content of heteroatoms is revealed by the XPS measurements. Accordingly, number of active sites

$$= \left(W_N \times \frac{1\ mmol}{14.004\ mg} + W_p \times \frac{1\ mmol}{30.974\ mg}\right) \times 0.378\ mg\ cm^{-2} \times 6.022 \times 10^{20}\ sites\ mmol^{-1}$$

Where W_N is the mass content of N, and W_P is the mass content of P.

References:

S2.H. W. Liang, S. Bruller, R. H. Dong, J. Zhang, X. L. Feng and K. Mullen, *Nat. Commun.*, 2015, **6**, 7992.

S3.J. N. Tiwari, S. Sultan, C. W. Myung, T. Yoon, N. N. Li, M. R. Ha, A. M. Harzandi, H. J. Park, D. Y. Kim, S. S. Chandrasekaran, W. G. Lee, V. Vij, H. J. Kang, T. J. Shin, H. S. Shin, G. Lee, Z. Lee and K. S. Kim, *Nat. Energy*, 2018, **3**, 773-782.

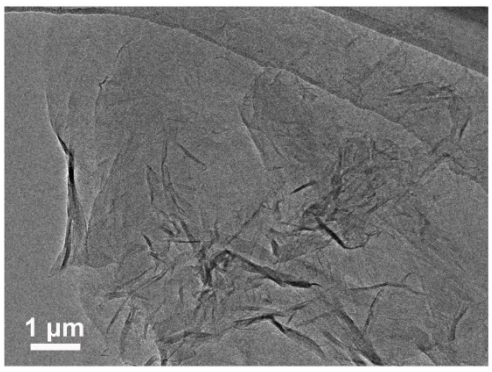

Fig. S31. The TEM image of G-12NP after 100 h durability tests.

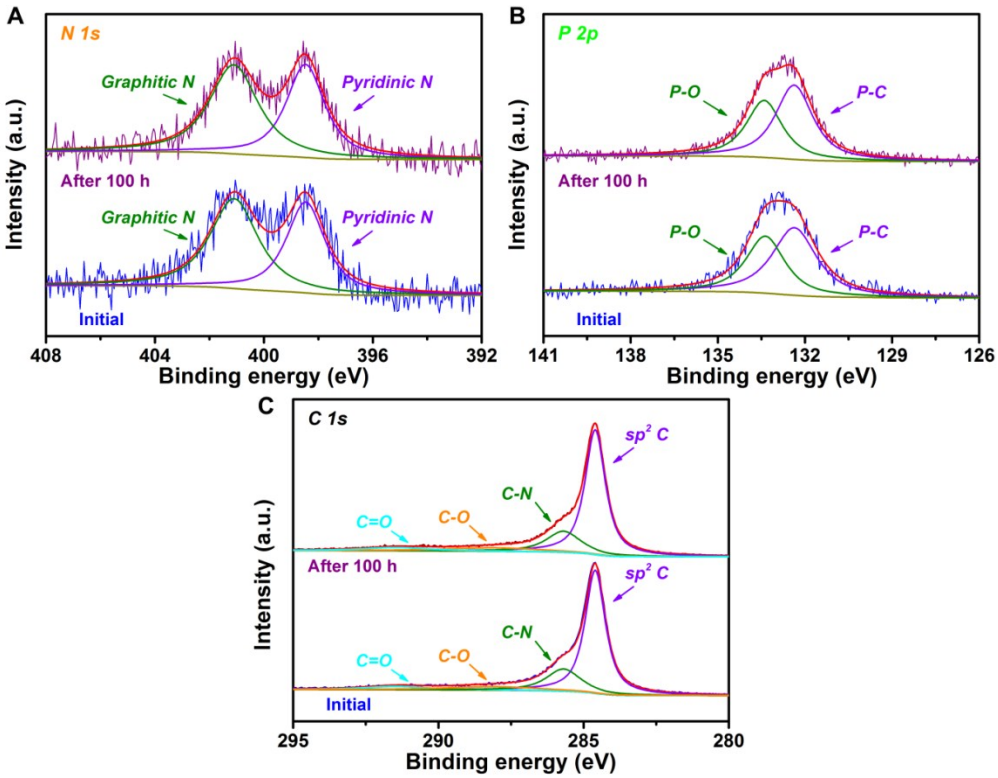

Fig. S32. The high-resolution N *1s* (A), P *2p* (B) and C *1s* (C) XPS spectra of G-12NP initially and after 100 h durability tests.[S4,S5]

References:

S4.J. T. Zhang, L. T. Qu, G. Q. Shi, J. Y. Liu, J. F. Chen and L. M. Dai, *Angew. Chem. Int. Ed.*, 2016, **55**, 2230-2234.

S5.Y. P. Zhu, Y. Jing, A. Vasileff, T. Heine and S. Z. Qiao, *Adv. Energy Mater.*, 2017, **7**, 1602928.

2. Supplementary Tables

Table S1. The typical FTIR and Raman bands of MP.

FTIR bands[S6,S7]		Raman bands[S8,S9]	
Wavenumber (cm^{-1})	**Assignment**	**Raman shift (cm^{-1})**	**Assignment**
3398	Asymmetric stretching absorptions of N-H	993	Ring breathing mode of triazine ring
3158	Symmetric stretching absorptions of N-H	928	PO_4 stretching
1673	Triazine ring vibration	699	Ring breathing mode and an in-plane deformation of triazine ring
1250	Stretching vibration of P=O	591	PO_4 bending in HPO_4^{2-} group
785	Triazine ring vibration	404	PO_4 bending in $H_2PO_4^{2-}$ group

References:

S6.L. Liu, Z. Z. Wang and X. Y. Xu, *J. Appl. Polym. sci.*, 2017, **134**, 45234.

S7.Z. H. Zheng, T. Yang, B. N. Wang, B. B. Qu and H. Y. Wang, *Polym. Int.*, 2015, **64**, 1275-1288.

S8.I. Liascukiene, M. Ben Salah, R. Sabot, P. Refait, L. Dhouibi, C. Methivier, J. Landoulsi and M. Jeannin, *Appl. Surf. Sci.*, 2018, **434**, 561-572.

S9.J. M. Li, Y. Yang and D. Qin, *J. Mater. Chem. C*, 2014, **2**, 9934-9940.

Table S2. Comparison of HER performance of G-12NP with the reported NHDG and other types of metal-free catalysts in 0.5 M H_2SO_4.

Catalysts	Substrate	η@10 mA·cm^{-2} (mV)	Tafel slope (mV/dec)	Reference
G-12NP	**GCE**	**106**	**67.3**	**This work**
N doped G	GCE	~580	133.8	*Chem. Commun. 2018, 54, 13726.*
B, S codoped G	GCE	230	72	*Angew. Chem. Int. Ed. 2018, 57, 13302.*
N doped G	GCE	210	---	*ACS Energy Lett. 2018, 3, 1345.*
N, P codoped G	GCE	~500	88	*ChemistrySelect 2018, 3, 6814.*
3D S doped G	GCE	218	64	*J. Mater. Sci. 2018, 53, 7767.*
Amine functionalized N doped G	GCE	350	113	*Carbon 2018, 138, 169.*
P nanodot incorporated G	GCE	440	46	*J. Mater. Chem. A 2018, 6, 3141.*
g-C_3N_4@2D mesoporous G	GCE	219	53	*Adv. Funct. Mater. 2017, 27, 1606352.*
N, F codoped G	GCE	290	87	*Catal. Sci. Technol. 2017, 7, 2228.*
Plasma-etched N doped G	GCE	128	66	*Appl. Catal. A: General 2017, 529, 127.*
N doped G	GCE	~380	---	*ChemCatChem 2017, 9, 4049.*
N, S codoped G	Ni foam	298	75	*Int. J. Hydrogen. Energ. 2017, 42, 27004.*
N, S codoped G	GCE	~300	120	*Nature Energy 2016, 1, 16130.*
Plasma-etched S doped G	GCE	178	86	*Int. J. Hydrogen. Energ. 2016, 42, 4184.*
N, P, S tridoped G	GCE	240	90	*Adv. Mater. 2016, 28, 10644.*
Plasma-etched N, S codoped G	GCE	149	78	*Electrochimica Acta 2016, 219, 781.*
B, N codoped G	GCE	216	92	*J. Mater. Chem. A 2016, 4, 16469.*
N, S codoped G	GCE	276	81	*Angew. Chem. Int. Ed. 2015, 54, 2131.*
N, P codoped G	GCE	213	79	*J. Mater. Chem. A 2015, 3, 12642.*
g-C_3N_4/N, P codoped G	GCE	340	90	*ChemCatChem 2015, 7, 3873.*
Holey N doped G	GCE	340	99	*Nano Energy 2015, 15, 567.*
N, P codoped G	GCE	~420	91	*ACS Nano 2014, 8, 5290.*
C_3N_4@N doped G	GCE	~240	51.5	*Nat. Commun. 2014, 5, 3783.*
B doped G	GCE	470	99	*Catal. Sci. Technol. 2014, 4, 2023.*

g-C_3N_4 nanoribbon/G	GCE	207	54	*Angew. Chem. Int. Ed. 2014, 53, 13934.*
N doped G	GCE	240	109	*Sci. Rep. 2014, 4, 7557.*
Defect-rich and ultrathin N doped carbon nanosheet	GCE	90	43	*Energy Environ. Sci. 2019, 12, 322.*
N doped CNT	GCE	360	118	*Catal. Lett. 2019, 149, 486.*
3D porous N doped carbon	GCE	143	64.3	*ChemCatChem 2018, 10, 5194.*
Pyrazine-incorporated graphdiyne	GCE	275	75	*J. Mater. Chem. A 2018, 6, 22189.*
Maleimide edge-functionalized G	GCE	420	110	*ChemistrySelect 2018, 3, 13070.*
Hexagonal BN-G	GCE	~390	---	*Phys. Chem. Chem. Phys 2018, 20, 15007.*
C_3N_4 quantum dot@G	GCE	110	53	*ACS Catal. 2018, 8, 3965.*
N functionalized CNT	GCE	250	---	*ChemCatChem 2018, 10, 3872.*
Graphite carbon nitride/B doped G	GCE	260	90	*Nanotechnology 2018, 29, 345705.*
3D G network	Si substrate	107	64	*Angew. Chem. Int. Ed. 2018, 57, 192.*
Ethylenediamine-functionalized multiwalled CNT	GCE	350	116	*Electrocatalysis 2018, 9, 573.*
NBC-ternary nanosheet	GCE	590	205	*Appl. Surf. Sci. 2018, 448, 618.*
CN_x@N doped G	GCE	193	54	*ChemElectroChem 2017, 4, 2643.*
N doped carbon	GCE	276	94	*J. Mater. Chem. A 2017, 5, 6025.*
3D CNT	GCE	~300	---	*ACS Catal. 2017, 7, 2676.*
S doped g-C_3N_4	GCE	186	84	*ACS Nano 2017, 11, 6004.*
Covalent organic polymer	GCE	250	106	*ACS Catal. 2017, 7, 6120.*
N, S codoped carbon nanosheet	GCE	290	76.9	*ACS Nano 2017, 11, 7293.*
Pyrene-porphyrin-based crystalline covalent organic framework	GCE	380@5	116	*ACS Appl. Mater. Interfaces 2017, 9, 23843.*
N doped graphitic carbon sheet	CC	320	198	*Int. J. Hydrogen. Energ. 2017, 42, 14390.*
Defect-rich, N, B codoped graphitic carbon nanocage	GCE	175.3	---	*Nano Energy 2017, 42, 334.*
S doped C_3N_4	GCE	145	51	*J. Mater. Chem. A 2016, 4, 12205.*
Horizontally-aligned CNT and G	GCE	420	121	*Carbon 2016, 107, 739.*
Acid treated multiwalled CNT	GCE	~180	71.3	*ACS Appl. Mater. Interfaces 2016, 8, 35513.*
Defective activated carbon	GCE	334	66	*Chem. Commun. 2016, 52, 8156.*
G nanostripe	GCE	560	85.3	*Angew. Chem. Int. Ed. 2016, 55, 13965.*

N doped carbon nanosheet	GCE	137	131.6	*Electrochimica Acta 2016, 215, 223.*
N, S codoped CNT	GCE	~270	126	*Chem. Eur. J. 2016, 22, 10326.*
BC_7N_2	GCE	70@20	100	*Energy Environ. Sci. 2016, 9, 95.*
Defect G	GCE	150	55	*Adv. Mater. 2016, 28, 9532.*
S-C_3N_4/CNT/CF	CF	236	81.6	*J. Mater. Chem. A 2016, 4, 12878.*
N, P codoped carbon network	GCE	163	89	*Angew. Chem. Int. Ed. 2016, 55, 2230.*
N, P codoped CF	GCE	151	69	*J. Mater. Chem. A 2016, 4, 13726.*
2D supramolecular polymer	GCE	333	80.5	*Angew. Chem. Int. Ed. 2015, 54, 12058.*
N, S codoped porous carbon	GCE	100	57.4	*J. Mater. Chem. A 2015, 3, 8840.*
N, S codoped carbon nanosheet	GCE	120	67.8	*Nano Energy 2015, 16, 357.*
C_3N_4 nanolayer@N doped G	GCE	80	49.1	*ACS Nano 2015, 9, 931.*
N, P codoped porous carbon	GCE	204	58.4	*J. Mater. Chem. A 2015, 3, 7210.*
Activated CNT	GCE	220	71.3	*Chem. Commun. 2014, 50, 9340.*

Abbreviations: G = Graphene; GCE = Glassy carbon electrode; CC = Carbon cloth; CF = Carbon fiber; g-C_3N_4 = graphitic-C_3N_4; CNT = Carbon nanotube.

Table S3. Comparison of HER performance of G-12NP with recently reported metallic catalysts in 0.5 M H_2SO_4.

Catalysts	Substrate	η@10 mA·cm^{-2} (mV)	Tafel slope (mV/dec)	Reference
G-12NP	**GCE**	**106**	**67.3**	**This work**
G-supported single atom Co	GCE	230	99	*Adv. Energy Mater. 2019, 9, 1803689.*
Co−N/C	GCE	~202	82	*ACS Catal. 2019, 9, 83.*
Co/PCN	GCE	89	52	*Nat. Catal. 2019, 2, 134.*
Monolayer MoS_2	GCE	200	75	*Nat. Commun. 2019, 10, 1348.*
Ni-doped FeP/carbon	GCE	72	54	*Sci. Adv. 2019, 5, eaav6009.*
MoS_2/rGO	GCE	186	49	*Small 2019, 15, 1804903.*
Co-Fe-P nanotube	GCE	66	72	*Nano Energy 2019, 56, 225.*
Meso-CoS_2	GCE	110	52	*ACS Catal. 2019, 9, 456.*
WS_2/Ni_5P_4-Ni_2P	Ni foam	94	74	*Nano Energy 2019, 58, 193.*
17.7 wt% Ir/Si nanowire	GCE	22	20	*ACS Nano 2019, 13, 2786.*
N, P codoped MoS_2	CC	116	58.4	*Nano Energy 2019, 58, 862.*
$[Mo_2O_2(\mu\text{-}S)_2(S_2)_2]^{2-}$	GCE	~114	~52	*Nat. Commun. 2019, 10, 370.*
CoS|Ni|P nanosheet	Ni foam	41	45.2	*Small 2019, 15, 1804272.*
RuB_2	GCE	17	38.9	*Adv. Energy Mater. 2019, 9, 1803369.*
W_2C	GCE	~268	65	*Small 2019, 15, 1900248.*
Amorphous MoS_x	GCE	145	40	*Adv. Funct. Mater. 2019, 29, 1806229.*
Ni@N doped carbon@MoS_2	GCE	82	47.5	*Small 2019, 15, 1804545.*
Ni_2P/MoS_2/N doped CNT	GCE	91.5	39.5	*Adv. Funct. Mater. 2019, 29, 1809151.*
CoP/NiCoP/N doped carbon	GCE	60	64	*Adv. Funct. Mater. 2019, 29, 1807976.*
Ultrafine Mo_2C particle	GCE	62	57	*Small 2019, 15, 1900358.*
Single-atomic Co/N doped carbon	GCE	137	52	*Proc. Natl. Acad. Sci. USA 2018, 115, 12692.*
Ru@G	GCE	13	30	*Adv. Mater. 2018, 30, 1803676.*
2D $MoS_{2-x}O_x$	GCE	~255	67	*Nat. Chem. 2018, 9, 810.*
Ir@cage-like organic network	GCE	13.6	27	*Adv. Mater. 2018, 30, 1805606.*

MoSSe nanodot	GCE	140	40	*Adv. Mater. 2018, 30, 1705509.*
p-$(CH_3CH_2)_2$NPh-MoS_2	GCE	~348	~75	*J. Am. Chem. Soc. 2018, 140, 441.*
Co doped $WS_2/W_{18}O_{49}$ nanotube	FTO	210	49	*Energy Environ. Sci. 2018, 11, 2270.*
Core-shell N-C-NiFe nanoparticle	CW	179	52.8	*Adv. Energy Mater. 2018, 8, 1801289.*
Multi-channel carbon matrix nanofibers@MoS_2-Ni	GCE	161	81	*Adv. Funct. Mater. 2018, 8, 1807086.*
S, N codoped Fe_2N	GCE	123	90	*Small 2018, 14, 1803500.*
Defect G trap atomic Ni species	GCE	70	31	*Chem 2018, 4, 285.*
Mo_2N–Mo_2C/holey reduced GO	GCE	157	55	*Adv. Mater. 2018, 30, 1704156.*
CoP@N doped carbon/N doped G	GCE	135	59.3	*Small 2018, 14, 1702895.*
Monolayer MoS_2	GCE	126	67	*Adv. Energy Mater. 2018, 8, 1800734.*
Ni-Co-P nanosheet	GCE	80	---	*J. Am. Chem. Soc. 2018, 140, 5241.*
$MoSe_2$ flake/single-wall CNT	GCE	100	63	*Adv. Energy Mater. 2018, 8, 1703212.*
N-$MoSe_2$/TiC-C	TiC-C	106	32	*Adv. Mater. 2018, 30, 1802223.*
Ni_2P@N doped carbon nanofiber	GCE	63.2	56.7	*Angew. Chem. Int. Ed. 2018, 57, 1963.*
$Mo_{0.5}W_{0.5}S_2$	GCE	138	55	*ACS Catal. 2018, 8, 9529.*
Ultrathin CoP nanosheet aerogel	GCE	113	72	*Small 2018, 14, 1802824.*
V doped Co_4N nanosheet	GCE	37	44	*Angew. Chem. Int. Ed. 2018, 130, 5170.*
Mo/Co@N doped carbon	GCE	187	148	*Small 2018, 14, 1704227.*
MoP/N doped G	GCE	94	50.1	*Small 2018, 14, 1800667.*
1T-MoS_2	GCE	230	45	*ACS Energy Lett. 2018, 3, 7.*
PANI nanodots decorated CoP nanowire	CFP	~50	34.5	*J. Am. Chem. Soc. 2018, 140, 5118.*
$Er_2Si_2O_7$:IrO_2	GCE	130	49	*ACS Catal. 2018, 8, 8830.*
Ru single atoms@phosphorus nitride imide nanotube	GCE	24	38	*Angew. Chem. Int. Ed. 2018, 57, 9495.*
WS_2/WO_3/rGO	GCE	113	37	*Nano Energy 2018, 47, 66.*
1T'-Phase $ReS_{2x}Se_{2(1-x)}$	GCE	84	50.1	*J. Am. Chem. Soc. 2018, 140, 8563.*
Thiomolybdate $[Mo_3S_{13}]_2$-cluster	GCE	137	51	*ACS Catal. 2018, 8, 5221.*
Silk-cocoon structured CoS_x	GCE	42	41	*Energy Environ. Sci., 2018, 11, 2467.*
NPNi-MoS_2/rGO	GCE	205	71.3	*ACS Catal. 2018, 8, 8107.*

Ni/WC@N doped carbon sheet	GCE	53	43.5	*Energy Environ. Sci. 2018, 11, 2114.*
CoP/Ni_5P_4/CoP microsheet array	Ni foam	85	43	*Energy Environ. Sci. 2018, 11, 2246.*
Cu_2Se sheet	Cu foam	~212	32	*ACS Catal. 2018, 8, 5686.*
N, P codoped carbon-encapsulated ultrafine MoP nanocrystal/MoP cluster	CC	74	50	*Adv. Funct. Mater. 2018, 28, 1801527.*
Co_9S_8/MoS_2	GCE	97	71	*Adv. Mater. 2018, 30, 1707301.*
MoP/CNT	GCE	83	60	*Adv. Funct. Mater. 2018, 28, 1706523.*
2D $MoSe_2$ nanosheet	GCE	126	38	*Small 2018, 14, 1704150.*
Mo/β-Mo_2C	GCE	89	70.7	*ACS Energy Lett. 2018, 3, 341.*
Li^+ activated WSe_2 nanoflower	CFP	243	---	*Nano Lett. 2018, 18, 2329.*
Co-Co_2P@N, P doped carbon/rGO	GCE	61.5	42.5	*Adv. Funct. Mater. 2018, 28, 1801332.*
Co@N-CNTs@rGO	GCE	87	55	*Adv. Mater. 2018, 30, 1802011.*
MoS_2/hydrogenated G	GCE	124	41	*ACS Catal. 2018, 8, 1828.*
Mo_2B_4	GCE	~260@3.5	80	*J. Am. Chem. Soc. 2017, 139, 12915.*
N-doped 1T-2H $MoSe_2$/G	GCE	98	62	*Adv. Mater. 2017, 29, 1700748.*
$W_xMo_{1-x}S_2$/rGO film	GCE	96	38.7	*ACS Nano 2017, 11, 5103.*
2D WC single crystal/G	GCE	120	38	*Nano Energy 2017, 33, 356.*
RuP_2@N, P codoped carbon	GCE	38	38	*Angew. Chem. Int. Ed. 2017, 56, 11559.*
Zn-MoS_2	GCE	~140	51	*J. Am. Chem. Soc. 2017, 139, 15479.*
Crumpled MoS_2	CC	193	66	*Adv. Mater. 2017, 29, 1703863.*
Carbon-shell-coated FeP nanoparticle	GCE	71	52	*J. Am. Chem. Soc. 2017, 139, 6669.*
PtO_x/TiO_2	GCE	~125	40	*Energy Environ. Sci. 2017, 10, 2450.*
MoB_2	GCE	~240@3.5	75	*Angew. Chem. Int. Ed. 2017, 56, 5575.*
α-MoB_2	GCE	149	---	*J. Am. Chem. Soc. 2017, 139, 12370.*
WC@N doped carbon	GCE	51	49	*J. Am. Chem. Soc. 2017, 139, 5285.*
1T-$MoSe_2$ nanosheet	GCE	152	52	*Adv. Mater. 2017, 29, 1700311.*
Monolayer MoS_2	GCE	~220	---	*J. Am. Chem. Soc. 2017, 139, 16194.*
Monolayer MoS_2	GCE	~77	~60	*Adv. Mater. 2017, 29, 1701955.*
Pd/Cu-Pt nanoring	GCE	22.8	28	*Angew. Chem. Int. Ed. 2017, 56, 16047.*
Ternary $NiCo_2P_x$ Nanowire	Carbon felt	104	58.8	*Adv. Mater. 2017, 29, 1605502.*

$Ni_{0.89}Co_{0.11}Se_2$	Ni foam	52	39	*Adv. Mater. 2017, 29, 1606521.*
MoS_2	Cu foil	~100	39	*Sci. Adv. 2017, 3, e1602215.*
$Ru@C_2N$	GCE	13.5	30	*Nat. Nanotech. 2017, 12, 441.*
1T-phase MoS_2	GCE	~300@5	58	*Adv. Mater. 2016, 28, 10033.*
$MoSe_2$*/Mo core-shell nanoscrew*	Mo substrate	166	34.7	*Adv. Mater. 2016, 28, 9831.*
MoO_x/MoS_2 *Core-Shell Nanotubular*	GCE	259	63	*Angew. Chem. Int. Ed. 2016, 55, 12252.*
Metallic-phase MoS_2	GCE	175	41	*Nat. Commun. 2016, 7, 10672.*
Activated-Ni-Carbon catalyst	GCE	34	41	*Nat. Commun. 2016, 7, 10667.*
W_2C *nanoparticle*	GCE	123	45	*Nat. Commun. 2016, 7, 13216.*
Mn doped $CoSe_2$*ultrathin nanosheet*	GCE	174	36	*J. Am. Chem. Soc. 2016, 138, 5087.*
Hollow $Zn_{0.3}Co_{2.7}S_4$	GCE	80	47.5	*J. Am. Chem. Soc. 2016, 138, 1359.*
$MoS_{0.94}P_{0.53}$	GCE	~150	57	*Adv. Mater. 2016, 28, 1427.*
$WS_2/WO_{2.9}$	Graphite paper	~110	36	*Adv. Mater. 2016, 29, 1603617.*
Ni−C−N nanosheet	GCE	60.9	32	*J. Am. Chem. Soc. 2016, 138, 14546.*
Se-enriched $NiSe_2$ *nanosheet array*	CF	117	32	*Angew. Chem. Int. Ed. 2016, 55, 6919.*
$CoMoS_3$ *hollow prism*	GCE	171	56.9	*Adv. Mater. 2016, 28, 92.*
MoS_2 *with S-vacancy*	GCE	170	60	*Nat. Mater. 2016, 15, 48.*
Mo–W–P	CC	~80	52	*Energy Environ. Sci. 2016, 9, 1468.*
$Cu_7S_4@MoS_2$	GCE	133	48	*Angew. Chem. Int. Ed. 2016, 55, 6502.*
$MoS_{2(1-x)}Se_{2x}/NiSe_2$	GCE	69	42.1	*Nat. Commn. 2016, 7, 12765.*
Rh_2S_3	GCE	137	44	*Energy Environ. Sci. 2016, 9, 850.*
Mo_2C*@N, P codoped carbon*	GCE	34	33.6	*Nat. Commn. 2016, 7, 11204.*
P_8W_{48}*/rGO*	GCE	28	38	*Energy Environ. Sci. 2016, 9, 1012.*
Co-N-doped G	GCE	~147	82	*Nat. Commun. 2015, 6, 8668.*
Co−C−N	GCE	138	55	*J. Am. Chem. Soc. 2015, 137, 15070.*
WO_2*−carbon mesoporous nanowire*	GCE	58	46	*J. Am. Chem. Soc. 2015, 137, 6983.*
Mo_2C*@N-doped carbon*	GCE	~120	60	*Angew. Chem. Int. Ed. 2015, 54, 10752.*
CoN_x/C	GCE	133	57	*Nat. Commun. 2015, 6, 7992.*
Fe-Ni-S	GCE	105	40	*J. Am. Chem. Soc. 2015, 137, 11900.*
Mo_2C*@carbon*	GCE	78	41	*Angew. Chem. Int. Ed. 2015, 54, 14723.*

Edge-terminated MoS_2	GCE	149	49	*Nat. Commun. 2015, 6, 7493.*
MoCN	GCE	140	46	*J. Am. Chem. Soc. 2015, 137, 110.*
MoO_2@P-doped carbon-RGO	GCE	64	41	*Angew. Chem. Int. Ed. 2015, 54, 12928.*
H-MoS_2	GCE	167	98	*Adv. Mater. 2015, 27, 7426.*
Ni_5P_4-Ni_2P	Ni foam	120	79.1	*Angew. Chem. Int. Ed. 2015, 54, 8188.*
$Mo_{0.27}Ni_{2.4}$	GCE	75	45	*J. Am. Chem. Soc. 2015, 137, 15753.*
β-Mo_2C nanotube	GCE	172	62	*Angew. Chem. Int. Ed. 2015, 54, 15395.*
FeCo alloy@N-doped G	GCE	262	74	*Energy Environ. Sci., 2015, 8, 3563.*
VS_2 nanosheet	GCE	68	34	*Adv. Mater. 2015, 27, 5605.*
Ni-doped G	GCE	~150	45	*Angew. Chem. Int. Ed. 2015, 54, 14031.*
MoCx	GCE	142	53	*Nat. Commn. 2015, 6, 6512.*
Ni_5P_4	Ti-foil	23(1 M H_2SO_4)	33(1 M H_2SO_4)	*Energy Environ. Sci. 2015, 8, 1027.*
CoNi@N-doped carbon	GCE	142	105	*Angew. Chem. Int. Ed. 2015, 54, 2100.*
MoS_2/$CoSe_2$	GCE	68	36	*Nat. Commn. 2015, 6, 5982.*
$CoSe_2$ nanoparticle	CFP	137	41	*J. Am. Chem. Soc. 2014, 136, 4897.*
CoP/CNT	GCE	122	54	*Angew. Chem. Int. Ed. 2014, 53, 6710.*
CoP nanowire array	CC	67	51	*J. Am. Chem. Soc. 2014, 136, 7587.*
WS_2 nanosheet	GCE	142	70	*Energy Environ. Sci. 2014, 7, 2608.*
FeP nanoparticle	Ti-foil	50	~37	*ACS Nano 2014, 8, 11101.*
MoP	GCE	~130	54	*Energy Environ. Sci. 2014, 7, 2624.*
Cu_3P nanowire Array	CF	143	67	*Angew. Chem. Int. Ed. 2014, 53, 9577.*
MoP	GCE	125	54	*Adv. Mater. 2014, 26, 5702.*
FeP nanowire array	Ti-foil	55	38	*Angew. Chem. Int. Ed. 2014, 53, 12855.*
Oxygen-incorporated MoS_2	GCE	~170	55	*J. Am. Chem. Soc. 2013, 135, 17881.*
Defect-rich MoS_2	GCE	~200	50	*Adv. Mater. 2013, 25, 5807.*
MoS_2 nanosheet	RDE	187	43	*J. Am. Chem. Soc. 2013, 135, 10274.*
WS_2 nanosheet	GCE	~200	40	*Nat. Mater. 2013, 12, 850.*
Ni_2P nanoparticle	Ti-foil	~110	~46	*J. Am. Chem. Soc. 2013, 135, 9267.*
MoS_3/CNT	CPE	~250(1 M H_2SO_4)	41(1 M H_2SO_4)	*Energy Environ. Sci. 2012, 5, 6136.*
Mo_2C	RDE	~190	56	*Angew. Chem. Int. Ed. 2012, 51, 12703.*

Cu_2MoS_4	GCE	~300	95	*Energy Environ. Sci. 2012, 5, 8912.*
MoS_2/RGO	CFP	~150	~41	*J. Am. Chem. Soc. 2011, 133, 7296.*

Abbreviations: G = Graphene; GO = Graphene oxide; rGO = Reduced graphene oxide; GCE = Glassy carbon electrode; FTO = Fluorine doped tin oxide; CF = Carbon fiber; CFP = Carbon fiber paper; CW = Carbonized wood; CC = Carbon cloth; DE = Rotating disk electrode; CPE = Carbon paste electrode; CNT = Carbon nanotube.

Table S4. Parameters obtained by fitting the Nyquist plots of G-4NP, G-8NP, G-12NP, G-16NP, G-12NNP and G-12NPP using the equivalent circuit in ***Fig. S27***.

Samples	R_s (Ω)	R_1 (Ω)	CPE1 (F)	R_{ct} (Ω)	CPE2 (F)
G-4NP	2.23	0.79	2.21×10^{-12}	120.18	1.28×10^{-7}
G-8NP	2.22	0.55	3.18×10^{-12}	86.51	1.86×10^{-7}
G-12NP	2.15	0.38	4.61×10^{-12}	61.82	2.28×10^{-7}
G-16NP	2.16	0.41	4.26×10^{-12}	71.65	2.05×10^{-7}
G-12NNP	2.16	0.65	2.69×10^{-12}	101.31	1.33×10^{-7}
G-12NPP	2.17	0.60	2.92×10^{-12}	95.43	1.66×10^{-7}

Table S5. The detailed dosages of melamine and phosphoric acid in the process of synthesizing G-4NP, G-8NP, G-12NP, G-16NP, G-12NNP and G-12NPP, respectively.

Sample name	Melamine (mg)	Phosphoric acid (ml)
G-4NP	25	0.06
G-8NP	50	0.12
G-12NP	75	0.18
G-16NP	100	0.24
G-12NNP	100	0.12
G-12NPP	50	0.24